EMEP Report 1/2003
Date: August 2003

METEOROLOGISK INSTITUTT
Norwegian Meteorological Institute

Transboundary Acidification, Eutrophication and Ground Level Ozone in Europe

PART I

Unified EMEP Model Description.


EMEP/MSC-W: David Simpson, Hilde Fagerli, Jan Eiof Jonson, Svetlana Tsyro and Peter Wind


FMI Juha-Pekka Tuovinen

EMEP Status Report 2003

ISSN 0806-4520

Contents

Acknowledgements

The Unified EMEP model described in this report has benefi tted from the work and helpful discussions with a large number of colleagues.

Thanks are due to Dave Fowler, Ron Smith, Mark Sutton and colleagues from CEH, Edinburgh, for stimulating discussions which have improved the EMEP model's deposition routines over the last year. Thanks are also due to Lisa Emberson, Steve Cinderby (SEI, York), and Mike Ashmore (Univ. Bradford) for continued help and advice on the ozone deposition modelling. We would like to thank Sonja Vidič (MHSC in Zagreb) for providing information on effective stack heights. Rainer Friedrich, Stefan Reis and colleagues at the University of Stuttgart (IER) are thanked for providing data on the temporal variation and height distribution of emissions. Steffen Unger (GMD-FIRST, Berlin) has been of enormous help concerning the merging of the older EMEP models and in optimisation of the Unifi ed model.

We would like to thank our colleagues within the NMR Aerosol project for inspiring cooperation and constructive discussions on aerosol characterisation and modelling. In particular, we appreciate close cooperation with Markku Kulmula and Liisa Pirjola from the University of Helsinki, resulting in developing the aerosol dynamics module MM32. Thanks are due to Hans-Christen Hansson and Peter Tunved from the University of Stockholm for providing aerosol measurements and helping in results analyses. We are grateful to Swen Metzger (Max Planck Institute for Chemistry) for providing the gas/aerosol equilibrium model EQSAM.

At the Norwegian Meteorological Institute thanks are due to Vigdis Vestreng and Anna Benedictow for their work with the emissions and meteorological data-bases, Heiko Klein for the development of essential validation programs and programming support, Viel Ødegaard and colleagues at the Research Department for advice on meteorological parameters and the use of HIRLAM data, Anton Eliassen for expert help with the dispersion algorithms used in the model, as well as general support, and fi - nally to Leonor Tarrasón for enthusiastic leadership of the air pollution section and EMEP project. And of course to our former colleague Erik Berge who designed and

constructed the first EMEP Eulerian model.

The work documented here has been partly funded by the EU projects CARBOSOL and MERLIN and the NMR project on the long-range transport of particulate matter.

CHAPTER 1

Introduction

This report presents a detailed documentation of the EMEP MSC-W modelling system, as of August 2003 (latest model revision rv1.8). The formulations used by the model are given, along with details of input data-sets or appropriate references. The aim of this report is a concise description rather than discussion – the latter is left for more extended reports and publications on specific subjects.

The modelling tools previously available at EMEP MSC-W consisted of two main Eulerian models, the acidification model (MADE) of Berge and Jakobsen (1998), Olendrzyński et al. (2000), and the oxidant model (MACHO) of Jonson et al. (1997, 1998, 2001). Additionally there were two Lagrangian models, one for acidification (Hov et al. 1988, Iversen 1990) and one for photo-oxidants (Simpson 1993, 1995). After years of separate development these models had codes which differed from each other in numerous ways, and even different physical descriptions of processes such as dry deposition and aqueous chemistry.

The new unified modelling system has been designed to provide a common core to all MSC-W modelling activities, building upon one Eulerian model structure. In the new system the only differences between say the acidification and oxidant versions lie in the chemical equations solved, and in the various inputs associated with this (for example, emissions and boundary conditions).

We use the word "revision" to denote the state of progress of the whole modelling system. Table 1.1 summarises some of the revisions used for important projects, and places these these different model versions in context. Revision rv1.7 was used for the model evaluation work reported in the accompanying EMEP Report 1/2003 Part II. Revision rv1.8 reflects some small changes made while this documentation was underway, but the model results are very similar to rv1.7.

The EMEP modelling system allows several options with regard to the chemical schemes used, and the possibility of including aerosol dynamics. We use the word

Table 1.1: Recent Revisions of the Unified EMEP model system

Revision	Comments
rv1.1	Improved seasonal variation for dry deposition. Vertical exchange modified. Used for most TROTREP Calculations, initial CITY DELTA runs
rv1.2	Sub-grid deposition scheme, stomatal-flux calculation
rv1.6	Added co-deposition for SO_2,NH_3, explicit H2O2 loss for SO2. Used for final TROTREP Calculations and CITY DELTA project
rv1.7	'Mace-Head' correction to boundary conditions introduced. Common landuse for biogenic and deposition. Used in EMEP Report 1/2003, Part II
rv1.8	Consistency improvements

Notes: TROTREP: `http:/atmos.chem.le.ac.uk/trotrep`
CITY DELTA `http://rea.ei.jrc.it/netshare/thunis/citydelta`

Table 1.2: Summary of standard model versions, including number of advected species (N_{adv}) and of short-lived species (N_{sh}).

	N_{adv}	N_{sh}	Purpose and Comment
UNI-ACID	12	0	Simple chemistry for acidification, eutrophication, and primary particles
UNI-OZONE	56	15	Full oxidant chemistry, plus acidification, eutrophication, and primary particles
UNI-AERO	29	0	Dynamic aerosol physics (research model)

"version" to distinguish between the different possibilities. In principal, the new modelling system can run any chemistry with relatively little effort, but we have two standard chemistries, UNI-ACID and UNI-OZONE, derived from the earlier acidification and oxidant applications of the model. Additionally, the model version with aerosol dynamics is labelled UNI-AERO. Table 1.2 summarises these versions. For current policy runs, the UNI-OZONE chemistry is used as standard.

The core subroutines handling physics, meteorology and both the UNI-ACID and UNI-OZONE chemistries are derived from previous EMEP models and have been subject to extensive testing (e.g. Tarrasón, L. ed). These core-modules may now be regarded as relatively stable, and hence form the main focus of this report. The aerosol dynamics model (UNI-AERO) is comparatively very new to the EMEP model system and the data required to evaluate this model properly are only now becoming available (for example, proper evaluation would require emissions inventories to carry

information on number density and chemical composition of emissions - something which has hardly started in Europe). This UNI-AERO version of the model is therefore more of a research tool at present and thus more likely to change in future than the ACID and OZONE model versions.

Chapters 2–9 document the core modules of the Unified EMEP model, including physical structure, emissions, background concentrations and details of the ACID and OZONE versions. Appendix A presents the current status of the aerosol dynamics model. Appendix B presents new methodologies needed for calculating vegetation-specific AOTx values and stomatal flux of ozone.

1.1 Updates and Web-site

The Unified model has been developed and tested to such an extent that it is hoped that this report will serve as basic documentation for some years. A HTML version of this report will be available on the EMEP web-site (`http://www.emep.int`), along with supplementary information. However, the model will be of course be subject to change as improved methods are introduced. It is anticipated that these changes will be documented through updates to the web-documentation. It is recommended therefore that the web-site is always consulted in conjunction with this report.

CHAPTER 2

Physical Description of the Model

2.1 Domain and Model-Coordinates

The basic physical formulation of the EMEP model is unchanged from that of Berge and Jakobsen (1998). The model uses the same horizontal and vertical grid as the meteorological data (chapter 3). A polar-stereographic projection, true at 60°N, is used. Details of this projection and the conversion to and from latitude-longitude are given elsewhere (`http://www.emep.int`, also Posch et al. 2001, Appendix A). At 60° N the the grid-size is 50×50 km^2.

Figure 2.1 illustrates the horizontal domain and grid of the EMEP model. As illustrated here, the full model domain is larger than the official EMEP area. The relationship between the model coordinates and official EMEP coordinates is straightforward:

$$\begin{aligned} x_{mod} &= x_{off} + 35.0 \\ y_{mod} &= y_{off} + 11.0 \end{aligned} \tag{2.1}$$

The model is defined vertically with so-called σ coordinates:

$$\sigma = \frac{p - p_T}{p^*} \tag{2.2}$$

where $p^* = p_S - p_T$ and p, p_S and p_T are the pressure at level σ, at the surface, and at the top of the model domain (currently 100 hPa), respectively. The model currently uses 20 vertical levels, as illustrated in Figure 2.2. The model system uses an inverted vertical numbering coordinate, k, with values from $k = 1$ for the highest layer to $k = 20$ for the layer nearest the ground. Figure 2.3 shows the lowest two layers in this system, with the σ levels from Figure 2.2 as solid lines, and the 'mid'-layers for which

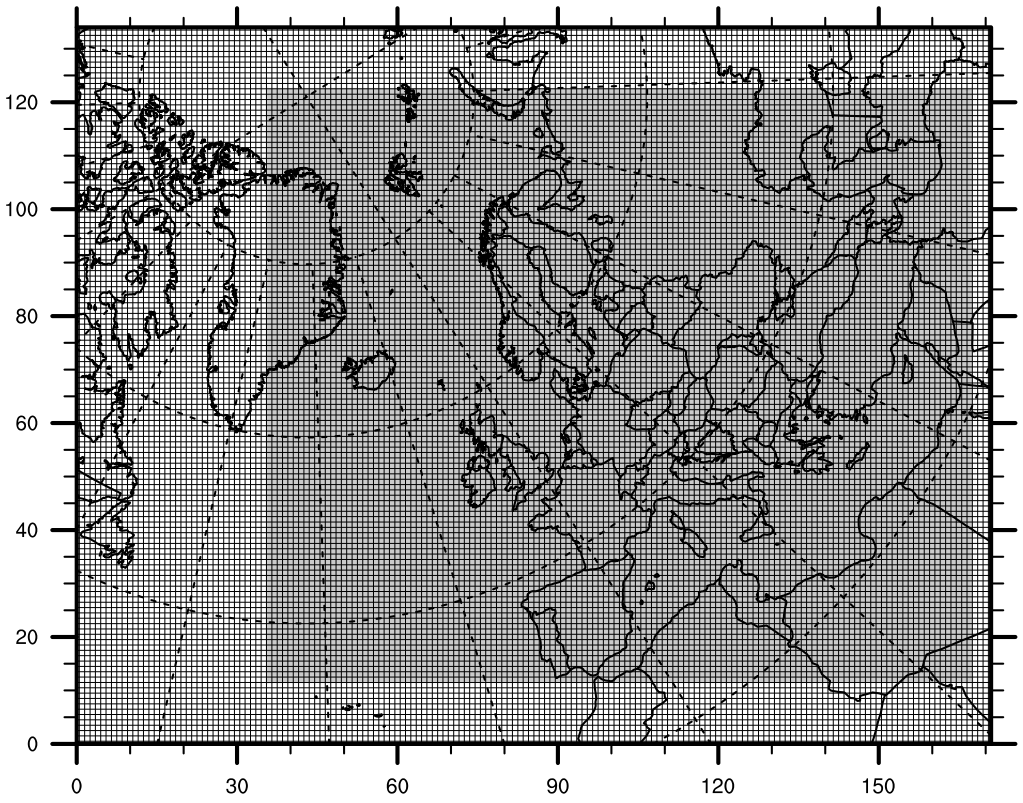

Figure 2.1: The EMEP Model Domain. The large area shows the full model domain and **model** coordinate system. The inner domain shows the official EMEP grid. The relationship between the official grid coordinates and the model grid coordinates is given in eqn [2.1].

meteorology is generally provided as dashed lines. Diffusion coefficients and vertical velocity, given by $\dot{\sigma}$ ($= d\sigma/dt$), are valid for the layer boundaries.

2.2 The continuity equation

If we let C represent the mixing ratio (kg/kg-air) of any pollutant, the continuity equation may we written

$$\frac{\partial}{\partial t}(Cp^*) = -m^2 \nabla_H \cdot \left(\frac{\mathbf{V}_H}{m}(Cp^*) \right) - \frac{\partial}{\partial \sigma}(\dot{\sigma} Cp^*) + \frac{\partial}{\partial \sigma}\left[K_\sigma \frac{\partial}{\partial \sigma}(Cp^*) \right] + \frac{p^*}{\rho} S \quad (2.3)$$

The first two terms on the right hand side represent a flux divergence formulation

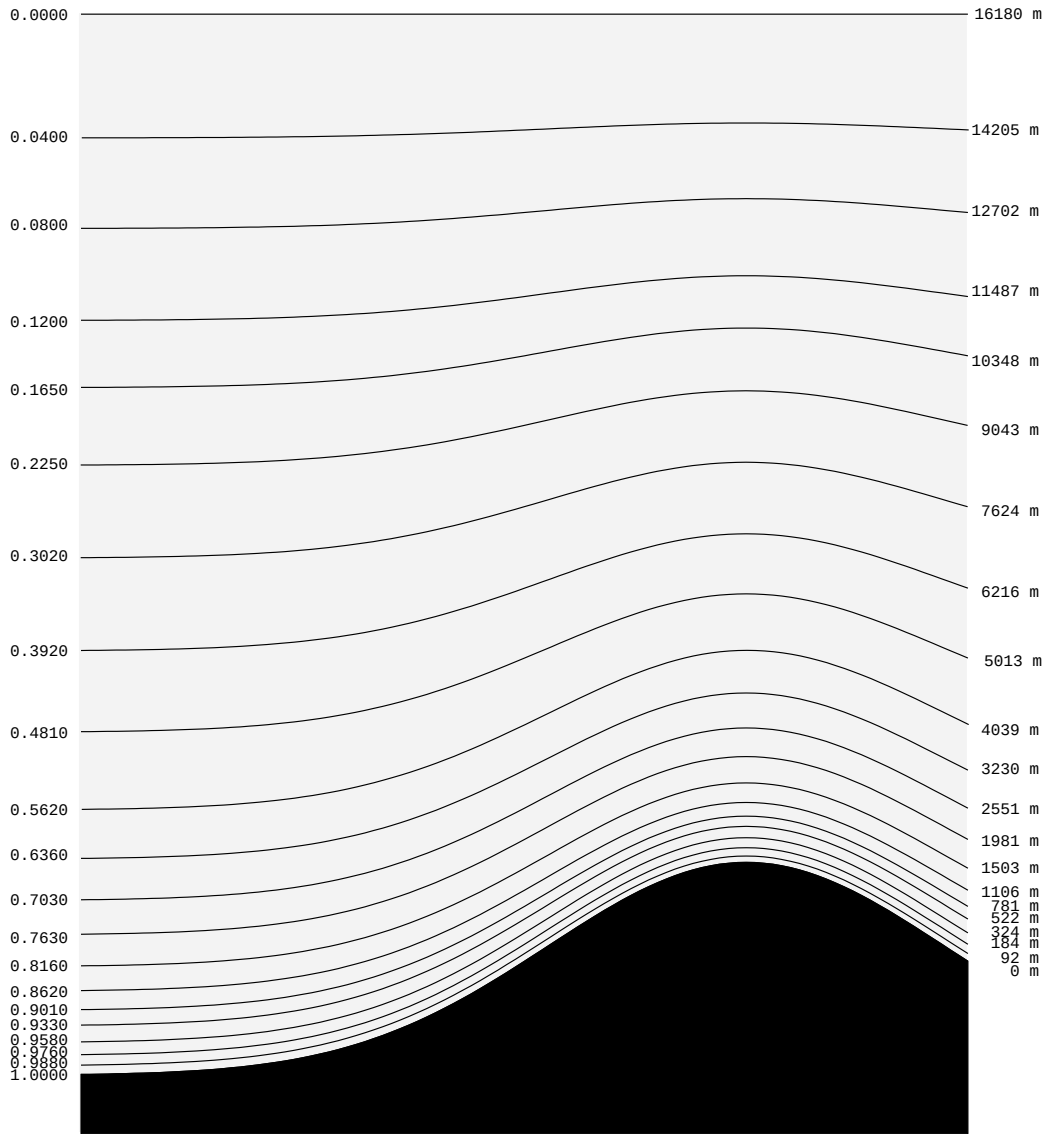

Figure 2.2: Vertical structure of the Unified EMEP model. The troposphere is represented in the model by 20 σ layers. Sigma values for the boundaries of each level are shown on the left hand side of the figure. The corresponding height above the ground, computed for a standard atmosphere, is given on the right-hand side.

of the advective transport. $\mathbf{V}_H$ and ∇_H are the horizontal wind vector and del operator respectively, and m is the map factor on a polar stereographic map projection.

The 3rd term on the right hand side of equation 2.3 represents the vertical eddy diffusion where g, ρ and K_σ are the gravitational acceleration, air density and vertical eddy diffusion coefficient respectively (in σ-coordinates). Horizontal eddy diffusion is not included in the model. S describes the chemical and other (deposition etc.) source

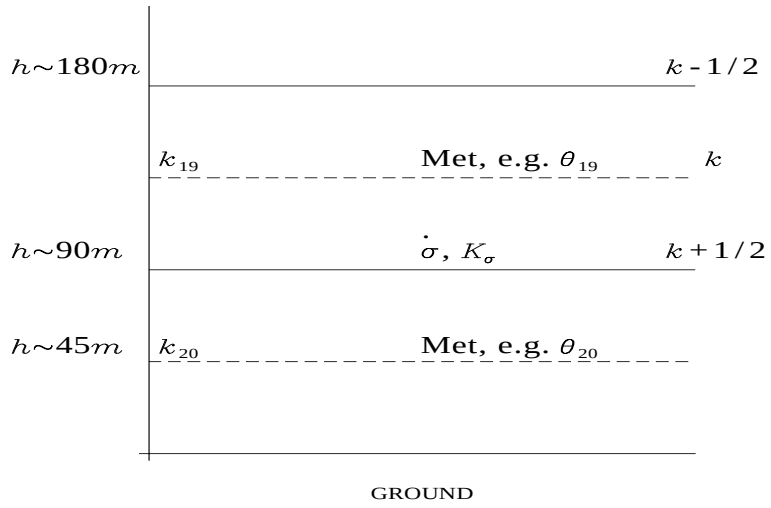

Figure 2.3: Lowest levels of the EMEP model, showing the layer boundaries at 90 m, 180 m (c.f. Figure 2.2) and the 'mid'-layers for which meteorology is generally provided.

and/or sink terms.

2.3 Advection

The numerical solution of the advection terms is based upon the scheme of Bott (1989a,b), as described in previous EMEP reports. The fourth order scheme is utilized in the horizontal directions. In the vertical direction a second order version applicable to variable grid distances is employed.

In our scheme the "air" (C=1 kg/kg-air) is also advected. After each advection step the new mixing ratios are found by dividing the result by the new "air concentrations":

$$C_x^{t+\Delta t} = \frac{(C_x p^*)^{t+\Delta t}}{(C_{air} p^*)^{t+\Delta t}} \tag{2.4}$$

where $(C_x p^*)^{t+\Delta t}$ is the result obtained with the Bott-scheme for component x after a timestep Δt . This method ensures that, starting with a constant mixing ratio, the result will also be be a constant mixing ratio, independently of the value of the wind fi elds.

The present model is not monotonic, because a monotonic fi lter may increase the numerical diffusion. However the scheme will exclude possible negative values of the mixing ratios. (For more details see Wind et al. 2002).

Some changes have recently been introduced in the advection algorithms, in order to allow flexibility in the choice of the grid resolution and meteorological data. This

work is described in detail in Wind et al. (2002), so only a brief outline is presented here.

2.3.1 Time step control

Numerical diffusion is one of the main limitations to the accuracy of the model. The size of the numerical diffusion will depend on the Courant number which in turn depend on the advection time step (Δt_{advec}). In order to optimize the size of the time step, an automatic control of the time step has been implemented in the model, allowing more than one elementary time step (Δt) within one advection time step if required. Given values of the mapping factor, m, grid dimension Δx and wind-speed u, a maximum value for the time-step Δt is derived:

$$\Delta t_{max} \leq \frac{\Delta x}{max(m_j^2\ u_j, 0) - min(m_j^2\ u_{j-1}, 0)}$$

This expression is evaluated over all grid cells, j. For the vertical direction the corresponding expression in σ coordinates is:

$$\Delta t_{max}^{vert} \leq \frac{\Delta \sigma_j}{max(\dot{\sigma_j}, 0) - min(\dot{\sigma_{j-1}}, 0)}$$

The time step is put to the same value for all cells in each horizontal direction although they can be different at different heights. The time step for the vertical advection can also be different from the time step in the horizontal directions, but all elementary time steps for the one dimensional advection have to be an integer fraction of Δt_{advec}.

2.4 Implementation of the model on a parallel computer

In order to produce results covering several years and several different situations, the model requires large computer resources. The program code is written in Fortran 90 and calculation are done at present on a SGI Origin 3800 supercomputer in Trondheim (Norway). The structure of the program is designed to allow for effi cient parallelization on a system with distributed memory. The communication between processors is based on GC package of subroutines (Generalized Communication, GC is an interface to most existing communication systems, Amundsen and Skålin (1995)) .

The horizontal grid is divided into a number of subdomains and each subdomain is assigned to a processor. Each processor holds only the data for its own subdomain. Because of this structure, the communication between the processors is kept to a minimum. Still the advection routines fundamentally require information to be passed

between processors. The input/output of data is also a limitation of the level of parallellity which can be achieved. The meteorological data is stored on disc and has to be read serially and distributed to all the nodes. Also the writing of results cannot be done entirely in parallel. Further details on the parallel architecture of the code can be found in Skålin et al. (1995).

The most CPU demanding part of the program is the chemistry module, because of the large number of chemical components and reactions. The chemical reactions have to be described for all the grid-cells and with a small time scales. However the chemistry is local and is therefore perfectly suited for parallelization. The deposition and wet scavenging processes have only vertical data dependencies and will therefore also parallelize effectively with the partitioning adopted in the program.

A typical run covering one year will require about 11 real time hours (352 CPU hours) on 32 MIPS R14000 1200 Mflops processors. The typical relative CPU usage of the different part of the program are: Chemistry 70% , Advection 10%, Meteorology and input/output 10%, Synchronisation between nodes 10%.

The code is written in such a way that the number of nodes can be chosen as input, but the relative CPU usage of the chemistry will decrease with increasing number of processors whereas the relative time used for the input/output and synchronisation will increase.

CHAPTER 3

Meteorology

The unified model uses 3-hourly resolution meteorological data from PARLAM-PS - a dedicated version of the HIRLAM (HIgh Resolution Limited Area Model) Numerical Weather Prediction (NWP) model, with parallel architecture (Sandnes Lenschow and Tsyro 2000, Bjørge and Skålin 1995). The PARLAM-PS data are archived over many years (currently back to 1980, though not continuously) and are typically produced one year after the current one (i.e. data for 2002 will be produced in 2003). The data produced are carefully checked and documented (Benedictow 2003).

3.1 PARLAM-PS Data

Table 3.1 summarises the PARLAM-PS meteorological fields currently used in the EMEP model. Most 3-D fields are provided at the centre of each model layer, thus we have 20 vertical fields (cf. Fig. 2.3). The vertical velocity, given by $\dot{\sigma}$, is provided at the layer boundaries. The horizontal location of meteorological data is ilustrated in Figure 3.1 for the south-west corner of the model domain. The horizontal winds (u and v) are given on a staggered grid (this is also the case with the vertical vind component $\dot{\sigma}$). All other variables (represented as q in the picture) are given in the centre of the grid.

Linear interpolation between the 3-hourly values is used to calculate values of these parameters at each advection step. A number of other parameters are derived from these, for example air density, ρ, and the stability parameters and boundary layer heights described below.

Solar radiation is also calculated at every time-step for the deposition calculations, and for photolysis rates, based upon instantaneous values of the solar zenith angle and the model's cloud cover. For these purposes, we define a total cloud fraction a_k for

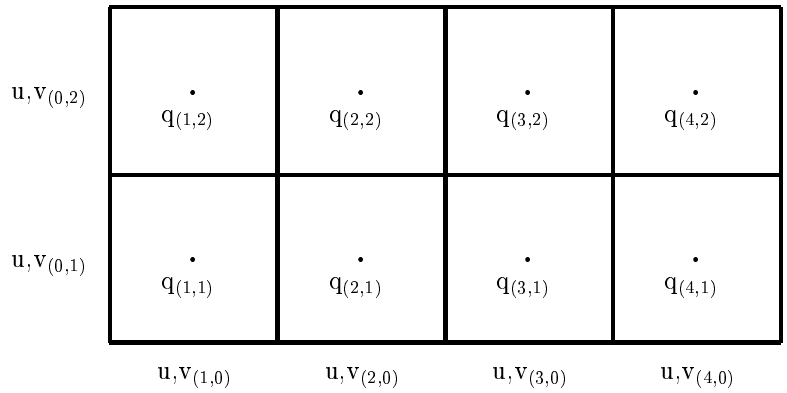

Figure 3.1: Horizontal placement of meteorological data, with wind components (u and v) and general variable q.

Table 3.1: Archived Meteorological Data Used in EMEP Model

Parameter	Unit	Description	Main Purpose
3D fields - for 20 σ levels			
u,v	m/s	Wind velocity components	Advection
q	kg/kg	Specific humidity	Chemical reactions, dry deposition
$\dot{\sigma}$	s^{-1}	Vertical wind in σ coordinates	vertical advection
θ	K	Potential temperature	Chemical reactions, eddy diffusion
CL	%	Cloud cover	Wet removal, photolysis
PR	mm	Precipitation	Wet and dry deposition
2D fields - for Surface			
Ps	hPa	Surface pressure	Surface air density
T_2	K	Temperature at 2m height	Dry deposition, stability
H	W m^{-2}	Surface flux of sensible heat	Dry deposition, stability
τ	M m^{-2}	Surface stress	Dry deposition, stability
LE	W m^{-2}	Surface flux of latent heat	Dry deposition

each model layer, such that a_k is equal to the maximum value of the local cloud cover from the 3-D fields for all layers above and including k (i.e. for $1...k$, see Fig. 2.3). Thus, at ground level we have a_{20} which is equal to the maximum cloud amount found in any layer above. This particular values, a_{20}, is also referred to as a_{CL} for clarity in the rest of this report.

3.2 Stability parameters

Atmospheric stability values and functions are derived using standard similarity theory profiles as given in say Garratt (1992). The Monin-Obukhov length is given by:

$$L = -\frac{T_2 \cdot u_*^3 \cdot \rho \cdot c_p}{k \cdot g \cdot H} \tag{3.1}$$

where u_* is the friction velocity, ($= \sqrt{\tau/\rho}$, m s^{-1}), c_p is the specific heat capacity of dry air (1005 J kg^{-1} K^{-1}), ρ is the air density (derived from surface pressure and temperature), k is von Karman's constant (0.41) and g is the gravitational acceleration (9.8 m s^{-2}). The sign here is consistent with H directed away from the surface (positive H gives unstable conditions). The similarity profile function for heat, Φ_h, is [1]:

$$\begin{aligned} \Phi_h(\zeta) &= (1-16\zeta)^{-1/2} && \text{if } \zeta < 0 \text{ (unstable)} \\ &= 1 + 5\zeta && \text{if } \zeta \geq 0 \text{ (stable)} \end{aligned} \tag{3.2}$$

where $\zeta = z/L$. The integral forms of the similarity functions for momentum (Ψ_m) and heat (Ψ_h) are:

$$\begin{aligned} \Psi_m(\zeta) &= \ln\left[\left(\frac{1+x^2}{2}\right)\left(\frac{1+x}{2}\right)^2\right] - 2.\arctan x + \frac{\pi}{2} && \text{if } \zeta < 0 \text{ (unstable)} \\ \Psi_h(\zeta) &= 2\ln\left[\frac{1+x^2}{2}\right] && \text{if } \zeta < 0 \text{ (unstable)} \\ \Psi_m(\zeta) &= \Psi_h(\zeta) = -5\zeta && \text{if } \zeta \geq 0 \text{ (stable)} \end{aligned} \tag{3.3}$$

where $x = (1-16\zeta)^{0.25}$. The local, bulk Richardson number in the layer of thickness Δz is defined as

$$Ri = \frac{g}{\theta} \cdot \frac{\left(\frac{\Delta\theta}{\Delta z}\right)}{\left(\frac{\Delta V_H}{\Delta z}\right)^2} = \frac{g \cdot \Delta z \cdot \Delta\theta}{\theta \cdot (\Delta V_H)^2} \tag{3.4}$$

where θ is potential temperature and V_H is the horizontal wind speed, so that $(\Delta V_H)^2 = (\Delta u)^2 + (\Delta v)^2$, and where for an arbitrary state variable q at model boundary level $k+1/2$, $\Delta q = q_k - q_{k+1}$ (c.f. Figure 2.3). Following Nordeng (1986), Pielke (2002), the critical Richardson number is given by:

$$Ri_c = A \cdot \left(\frac{\Delta z}{\Delta z_0}\right)^B \tag{3.5}$$

where A=0.115, B=0.175 and Δz_0=0.01 m.

[1] In earlier revisions of the EMEP model, including rv1.7, a slightly more complex formulation was used for Φ_h, based upon both Businger et al. (1971) and Iversen and Nordeng (1987)

3.3 Eddy Diffusion Coefficients

The turbulent diffusivity coefficients, K_z, are first calculated for the whole 3-D model domain on the basis of local Richardson numbers. The planetary boundary layer (PBL) height is then calculated using the methods of section 3.4. For stable situations (H <0) these K_z values are retained. For unstable situations, new K_z values are calculated for layers below the mixing height using the O'Brien interpolation (section 3.3.2).

To avoid non physically small exchange coefficients within the boundary layer, we introduce a minimum K_z for turbulent exchange between model layers below the mixing height, given by eqn [3.9] and evaluated at the top of the lowest model layer i.e. at z $\approx$ 90 meters.

In sigma coordinates, the diffusion coefficient has the following form:

$$K_\sigma = K_z \cdot \rho^2 \cdot \left(\frac{g}{p^*}\right)^2 \tag{3.6}$$

3.3.1 K_z, stable boundary layer and above the PBL

The initial calculation of the vertical exchange coefficients is given by

$$K_z = \begin{cases} 1.1(Ri_c - Ri)\, l^2\, |\Delta V_H/\Delta z|/Ri_c & Ri \le Ri_c \\ 0.001 & Ri > Ri_c \end{cases} \tag{3.7}$$

where l is the turbulent mixing length (m), and ΔV_H and Δz are as given above. The numerical values follow from the suggestions of Blackadar (1979) and Pielke (2002).

The turbulent mixing length, l, is parameterized according to:

$$\begin{aligned} l &= k \cdot z \quad & z \le z_m \\ l &= k \cdot z_m \quad & z > z_m \end{aligned}$$

where z is the height above the ground (actually above the displacement height, d, of PARLAM-PS) and z_m=200 m.

These values of K_z are applied to the free troposphere, above the PBL (mixing) height, and also for the stable PBL.

3.3.2 K_z, unstable boundary layer

In the unstable case, K_z is determined by the O'Brien (1970) profile:

$$\begin{aligned} K_z(z) = \quad & K_z(z_i) + \left(\tfrac{z_i - z}{z_i - h_s}\right)^2 \{K_z(h_s) - K_z(z_i) + (z - h_s)\cdot \\ & \left[\tfrac{\delta}{\delta z}(K_z(h_s)) + 2 \cdot \tfrac{K_z(h_s) - K_z(z_i)}{z_i - h_s}\right]\Big\} \qquad h_s \le z < z_i \end{aligned} \tag{3.8}$$

in which z_i is the mixing height and h_s is the height of the surface boundary layer (or the so-called constant flux layer). In the model calculation h_s is set to 4% of the mixing height z_i. From the similarity theory of Monin-Obukhov (see, e.g. Stull 1988, Garratt 1992) we have

$$K_z(z) = \frac{u_* \cdot k \cdot z}{\Phi\left(\frac{z}{L}\right)} \qquad z < h_s \tag{3.9}$$

where k is the von Karman constant and Φ is the stability function given in eqns [3.2].

3.4 Boundary Layer Height

Following Jakobsen et al. (1995), the height of the planetary boundary layer is estimated on the basis the NWP data and K_z calculations discussed above. Two different schemes are used, depending on the sign of the surface sensible heat flux.

$H < 0$, stable

When $H < 0$, the height of the PBL in this case is taken as the height of the lowest level where K_z, calculated using equations [3.4,3.5,3.7], is less than 0.1 m^2 s^{-1}. A minimum PBL height of 100 m is enforced.

$H >= 0$, unstable

If the PBL as a whole is unstable, the turbulent heat flux is directed upwards from the ground to the atmosphere. The heating from below will initiate convective mixing, which will cause the potential temperature in the PBL to be close to constant with height, following a dry adiabat. As the heating continues, the potential temperature will grow with time along with the thickness of the layer which is being convectively adjusted in the process.

We assume an adjustment time for distribution of heat throughout the PBL of one hour. Thus depending on the initial distribution of the potential temperature, the height of the unstable PBL is calculated as the thickness of the layer above the ground for which the change in the internal energy equals the heat input from the ground over one hour. Since both this thickness and the final temperature initially are unknown, this is done by stepping level by level in the vertical direction calculating the increment in internal energy for the layer (i.e. consisting of several layers) between the ground and the final level where the total change in internal energy equals the heat input from the ground. Finally, the PBL height is smoothed with a second order Shapiro filter in space (Shapiro 1970). The PBL height is not allowed to be less than 100 m or exceed 3000 m.

Examples of the mixing heights produced using this method can be found in Jakobsen et al. (1995), Fagerli and Eliassen (2002).

CHAPTER 4

Emissions

The emissions input required by EMEP model consists of gridded annual national emissions of sulphur dioxide (SO_2), nitrogen oxides (NO_x=NO+NO_2), ammonia (NH_3), non-methane volatile organic compounds (NMVOC), carbon monoxide (CO), and particulates ($PM_{2.5}$, PM_{10}). These emissions are provided for 10 anthropogenic source-sectors denoted by so-called SNAP codes. An eleventh source-sector exists in the official-submitted database, "Other sources and sinks", but this consists almost entirely of emissions from natural and biogenic sources. Official submitted emissions from such sources are not used in the modelling work, except for those from volcanoes. Section 4.2 below discusses the methods used for dealing with such emissions in the modelling framework. The procedures used for collecting anthropogenic emissions, filling-in gaps, and for spatial distribution can be found in Vestreng (2003). The emissions database is available from `http:\\www.emep.int`, and further details can be obtained at that site.

4.1 Anthropogenic Emissions

These emissions are distributed vertically according to a default distribution based upon the SNAP codes, as shown in Table 4.1. These distributions have been based upon plume-rise calculations performed for different types of emission source which are thought typical for different emission categories, under a range of stability conditions (Calculations by S. Vidič, Croatian Meteorological Institute, pers. comm.).

Emissions are distributed temporally according to monthly (Jan.-Dec.) and daily (Sun.-Sat.) factors derived from data provided by the University of Stuttgart (IER). These factors are specific to each pollutant, emission sector, and country, and thus reflect the very different climates and hence energy-use patterns in different parts of

Table 4.1: Vertical distribution of Anthropogenic Emissions: Percentage of each SNAP sector allocated to the vertical layers of the EMEP model (given as heights of layers, in m).

No.	Sources	Height of Emission Layer (m)					
		0–92	92–184	184–324	324–522	522–781	781–1106
1	Combustion in energy and transformation industries	0	0	8	46	29	17
2	Non-industrial combustion plants	50	50				
3	Combustion in manufacturing industry	0	4	19	41	30	6
4	Production processes	90	10				
5	Extraction and distribution of fossil fuels and geothermal energy	90	10				
6	Solvents and other product use	100					
7	Road transport	100					
8	Other mobile sources and machinery	100					
9	Waste treatment and disposal	10	15	40	35		
10	Agriculture	100					

Table 4.2: Day and night factors applied to anthropogenic emissions

SNAP:	1	2	3	4	5	6	7	8	9	10
Day	1.0	1.2	1.2	1.0	1.0	1.5	1.5	1.2	1.0	1.0
Night	1.0	0.8	0.8	1.0	1.0	0.5	0.5	0.8	1.0	1.0

Notes: emissions from international shipping assumed constant throughout the day.

Europe. Simple day-night factors are also applied, where day is defined as 0700-1800 local time, as given in Table 4.2.

VOC speciation

Speciation of VOC emissions are also specified separately for each source-sector, derived from the detailed United Kingdom speciation given in PORG (1993). The EMEP model uses a 'lumped-molecule' approach to VOC emissions and modelling, in which for example model species NC4H10 represents all C3+ alkanes, and o-xylene represents all aromatic species. Therefore, each of the species from the detailed UK

inventory has been assigned to one of the EMEP model's species according to its reactivity and chemical composition, as given in Andersson-Sköld and Simpson (1997). Although the exact VOC speciation used can be varied to suit particular emission scenarios (e.g. Reis et al. 2000), a default split is typically used, as given in Table 4.3.

Aircraft and Shipping

Seasonally averaged aircraft emissions are included for NO_x, from Gardner et al. (1997), giving 3-D fields for the whole model domain.

Emissions from local, domestic ships, are included in source sector 8 of the national databases. Emissions from international shipping are specified in a separate database.

As noted in Vestreng (2003) total releases of SO_2, NO_x, NMVOC and CO from ship traffic in the Atlantic Ocean, the North Sea, the Baltic Sea, the Black Sea and the Mediterranean are used as estimated by Lloyd's Register of Shipping. These emissions refer to 1990 and are disaggregated onto the EMEP grid. For PM_{10}, the emissions from shipping for the year 2000 from ENTEC (facilitated to EMEP from the European Commission, DG Environment) are included. These annual emissions are assumed constant through the year and day.

4.2 Biogenic emissions

NMVOC

Biogenic emissions of isoprene and (if required) monoterpenes are calculated in the model as a function of temperature and solar radiation, using the landuse datasets described in Chapter 5. Calculations are performed at every model timestep, using surface temperature (T_2) and photosynthetically active radiation (PAR), the latter being calculated from the model's solar radiation, modified by the total cloud fraction (a_{CL}, section 3.1). The basic system is based upon Guenther et al. (1993, 1994):

$$F = \epsilon D \gamma \tag{4.1}$$

Where F is the emission flux, ϵ is the emission rate for a particular species at a reference temperature of 30°C and photosynthetically active radiation of 1000 μmole m^{-2} s^{-1}, D is the biomass density, and γ is a dimensionless environmental correction factors representing the effects of temperature and PAR. The equations used for the γ-factors are as given in Guenther et al. (1993) and Simpson et al. (1995). The correction factor for temperature is illustrated in Figure 4.1.

The emission rates (ϵ) and biomass densities (D) of forest species are taken directly from Simpson et al. (1999). For our two vegetation categories seminatural vegetation

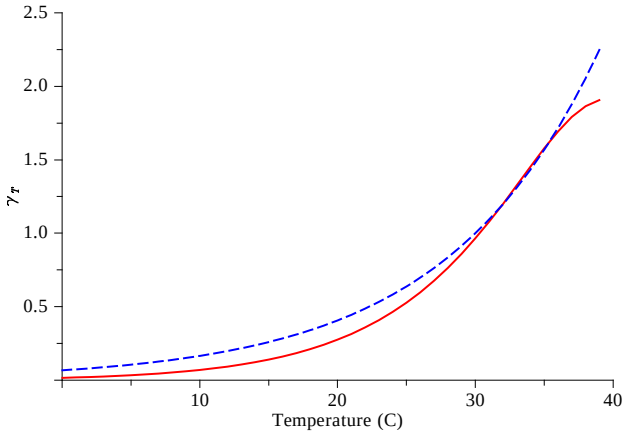

Figure 4.1: Temperature-variation of biogenic VOC emissions (γ-factor) as a function of temperature for isoprene (solid line) and monoterpenes (dashed line).

and Mediterranean scrub (SNL and MS, see chapter 5, Table 5.1) we adopt rates applied for similar species from Simpson et al. (1999), which for isoprene entails that D = 200 g m^{-2} dry-weight, and ϵ = 8 μg g^{-1} h^{-1}.

DMS

Biogenic emissions of di-methly-sulphide (DMS) are input as monthly average emission files, derived from Tarrasón et al. (1995). These DMS emissions are treated as SO_2 on input to the calculations.

Lightning

Emissions of NO_x from lightning are included as monthly averages on a T21 (5.65$\times$5.65°) resolution (Köhler et al. 1995). Both aircraft and lightning emissions are provided as 3-D fields for the whole model domain.

Volcanoes

Emissions of volcanoes are included for Italy, based upon the officially submitted data. Emissions are introduced as point sources, at a height determined by the height of each volcano.

Table 4.3: Default speciation of VOC emissions: Percentage (by mass) of each emissions (SNAP) sector allocated to model species.

SNAP	C2H6	NC4H10	C2H4	C3H6	OXYL	HCHO	CH3CHO	MEK	C2H5OH	CH3OH	UNREAC
1	12.97	30.57	16.10	8.55	2.77	1.76	1.93	0.773	22.29	0.387	1.907
2	12.97	30.57	16.10	8.55	2.77	1.76	1.93	0.773	22.29	0.387	1.907
3	12.97	30.57	16.10	8.55	2.77	1.76	1.93	0.773	22.29	0.387	1.907
4	0.146	0.971	1.88	0.00	0.828	0.00	0.00	0.355	93.47	0.079	2.273
5	0.0	82.01	2.41	10.96	2.39	0.00	0.00	0.0	2.239	0.0	0.0
6	5.36	35.99	0.00	0.00	27.30	0.00	0.00	3.666	19.97	0.0	7.717
7	4.86	30.87	8.63	7.00	36.76	1.64	1.06	0.0	8.75	0.0	0.447
8	5.70	18.00	12.00	4.60	10.60	5.90	4.00	0.0	39.20	0.0	0.0
9	48.41	48.41	0.00	0.00	0.00	3.18	0.00	0.0	0.0	0.0	0.0
10	12.97	30.57	16.10	8.55	2.77	1.76	1.93	0.773	22.29	0.387	1.907

Notes: For definition of model species (e.g. MEK, OXYL) see Chapter 7, Table 7.1.
Except for non-reacting species (UNREAC) which are excluded from the calculations.

CHAPTER 5

Landuse

Landuse data are required in the model, primarily for dry deposition modelling and for estimation of biogenic emissions. Previous versions of the EMEP Eulerian model actually had different data-sets to fulfill these two requirements. In the latest EMEP model revisions (rv1.7, rv1.8) the same landuse dataset is used for both purposes as described below.

As noted in chapter 2, the standard EMEP grid has a resolution of approx. 50×50 km^2. For each of these squares, the landuse databases give the fractional coverage of different vegetation types. This allows sub-grid modelling using a so-called mosiac approach - allowing for example ecosystem specific deposition estimates.

5.1 Landuse for Deposition Modelling

16 basic landuse classes have been identified for use in the new deposition module (chapter 8). These land-use classes are summarised in Table 5.1. Additional land-use classes are easily defined and indeed the specific categories "Wheat", "Potato" and "Beech" are assigned for critical level work, although with some special treatment (Appendix B).

For those vegetative landuse categories for which stomatal modelling is undertaken, the start and end of the growing season (SGS, EGS) must be specified. The development of leaf area index (LAI) within this growing season is modelled with a simple function as illustrated in Figure 5.1. The parameter values used for these LAI estimates are given in Table 5.1.

In principal, the EMEP model can accept landuse data from any dataset covering the whole of the domain and providing reasonable resolution of vegetation categories. Gridded data-sets providing these land-use categories across the EMEP domain have

Table 5.1: Land-use classes used in EMEP model, with default heights (h), albedo (α), growing-season and LAI-parameters

Code	Landcover	h (m)	α (%)	Growing season (SGS-EGS)	LAI parameters LAI_{min}	LAI_{max}	L_S	L_E
CF	Temperate/boreal coniferous forests	20†	12	All year	3.4	4.5	192	96
DF	Temperate/boreal deciduous forests	20†	16	90-270	3.5	5.0	56	92
NF	Mediterranean needle-leaf forests	15	12	All year	3.5	3.5	192	96
BF	Mediterranean broadleaf forests	15	16	All year	3.5	3.5	192	96
TC	Temperate Crops	1	20	105-197*	0.0	3.5	70	22
MC	Mediterranean Crops	2	20	105-197*	0.0	3.0	70	44
RC	Root Crops	1	20	130-250	0.0	4.2	35	65
SNL	Seminatural/Moorland	0.5	14	All year	2.0	3.0	192	96
GR	Grassland	0.5	20	All year	2.0	3.5	140	135
MS	Mediterranean scrub	3	20	All year	2.5	2.5	1	1
WE	Wetlands	0.5	14	All year	na	na	na	na
TU	Tundra	0.5	15	All year	na	na	na	na
DE	Desert	0	25	All year	na	na	na	na
W	Water	0	8	All year	na	na	na	na
I	Ice	0	70	All year	na	na	na	na
U	Urban	10	18	All year	na	na	na	na

Notes: For explanation of LAI parameters, see section 5.1 and figure 5.1.

† For boreal forests north of 60°N, height is reduced by 5% per degree extra latitude, down to a minimum of 6 m for 74°N and above.

∗ For these crops growing seasons vary with location. Currently we use a simple latitude-based function, although this will likely be replaced in future. Default values here apply to 50°N. SGS and EGS occur earlier at the rate of 3 days per degree latitude on moving south, or increase on moving north.

so far been based upon data from the Stockhom Environment Institute at York (SEI-Y) and from the Coordiniating Centre for Effects (CCE). The CCE dataset is based upon CORINE and PELCOM and is described in de Smet and Hettelingh (2001), along with some comparison to an earlier version of the SEI database. These datasets and the new SEI database (`www.york.ac.uk/inst/sei/APS/projects.html`) are also described in UNECE (2003). All datasets have advantages and disadvantages for EMEP purposes, so improvements are foreseen. As a first step, work is underway to merge the SEI and CCE data-sets.

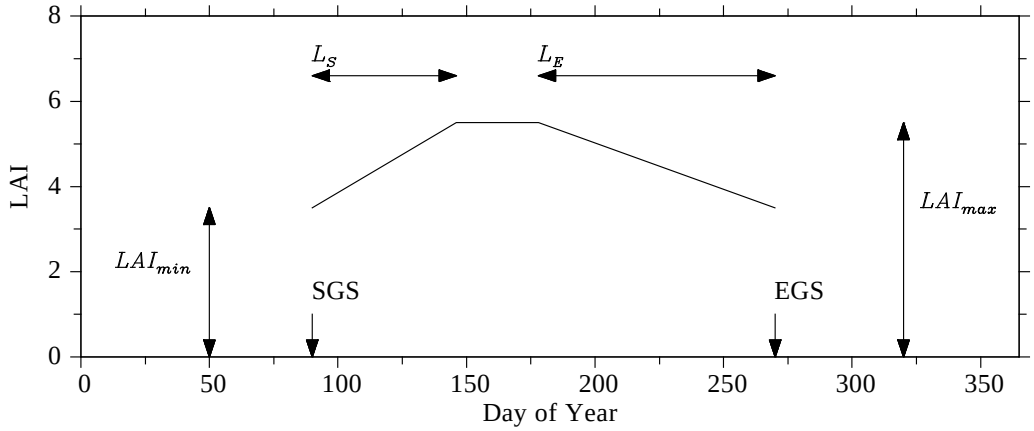

Figure 5.1: Schematic of LAI development and associated parameters. SGS and EGS are the start and end of the growing season, in day-numbers. L_S and L_E represent the length of the LAI-increase and decline periods, also in day-numbers. Maximum and minimum (within the growing season) LAI values are given by LAI_{max}, LAI_{min}.

5.2 Landuse for Biogenic Emissions

The above databases can provide gridded maps of say temperate coniferous forests or Mediterannean broadleaf forest, but contain little information on the actual species contained within these categories. The calculation of biogenic emissions requires such species information.

The species-specific landuse data required for biogenic NMVOC estimates are derived from the general landuse data base described above, making use of the categories coniferous and deciduous forest, and of seminatural vegetation and Mediterranean scrubs. These landuse categories were then disaggregated to specific species (Norway spruce, European oak, etc.), assuming the same fractions as found in the national totals summarised in Simpson et al. (1999).

CHAPTER 6

Initial and Boundary Conditions

Initial concentrations of major long-lived species are required in order to initialise model runs. Boundary conditions along the sides of the model domain and at the top of the domain are then required as the model is running. Additionally, we often need to specify concentrations of some species which are not explicitly included in the chemistry of interest, but that enter into reactions with some of the reacting chemical compounds ('background' species). In UNI-ACID, we use background concentrations for O_3, OH, CH_3COO_2 and H_2O_2. We refer here to all of these types of data as boundary conditions, or BCs.

Four methods of specifying boundary conditions are currently available:

i) 3-D Uni Provision of 3-D fields for whole domain from previous runs of the same or another version of the Unified model. (Self-assimilation)

ii) 3-D Obs. Provision of 3-D fields for whole domain from observational data sets, typically ozone-sondes for O_3.

iii) 3-D CTM Provision of 3-D fields for whole domain from other models, typically global chemical transport models (CTMs).

iv) Prescribed Simple functions are used to prescribe concentrations in terms of latitude and time-of-year, or time of day.

Method (i) is typically used when running one of the simpler Unified model versions. Thus, ozone and H_2O_2 have been calculated with the full UNI-OZONE chemistry, and fields stored for use in the UNI-AERO or UNI-ACID model.

Methods (ii) and (iii) allow great flexibility. A pre-processing program interpolates the data field of interest (e.g. derived from observations or global models) to the EMEP

Table 6.1: Default methods used to specify boundary conditions in Unified model versions. Angle brackets signifies 'background' species - see text.

Version	(i) 3D-Uni	(ii) 3-D Obs.	(iii) 3-D CTM	(iv) Prescribed
ACID	$<O_3>$,	-	-	NO, NO_2, SO_2, SO_4,
	$<H_2O_2>$	-	-	HNO_3, PAN, <OH>, $<CH_3COO>$
OZONE	-	O_3	-	As ACIDPM, + CO, HCHO, CH_3CHO, C_2H_6, C_4H_{10}, CH_4, H_2

50×50km^2 horizontal resolution and to the 20 vertical levels in the EMEP model. Currently, we use monthly averaged data fields with this method. However, the frequency of the update of the boundary conditions can be chosen freely, as long as the boundary condition field is provided for the same time period.

Method (iv) is used for those species where rather simple descriptions of boundary condition are sufficient. Despite the simplicity of this method, it has the advantage that the BCs can be based upon measurements and are easily understood.

Table 6.1 shows the default methods used for the different model versions. By default, UNI-OZONE uses method (ii) only for ozone, where a good description of BCs is essential (see section 6.1). Method (iii) is not used in any default setup, reflecting a decision to use observation-based methods as far as possible for routine EMEP modelling. However, this method allows interesting scenario studies (for example for future trend studies).

6.1 Ozone

Ozone is the gas where specification of accurate boundary conditions is most essential to a good model performance. This is due to the fact that ambient ozone levels in Europe are typically not much greater than the Northern hemispheric background ozone. Further, there is great interest in the modelling of quantities such as AOT40 (see Appendix B, section B.3), which expresses the amount by which O_3 levels exceed 40 pppb. As background tropospheric levels in many parts of Europe are also around 40 ppb, modelled values of AOT40 are extremely sensitive to uncertainties in the assumed background ozone.

Boundary conditions of ozone for UNI-OZONE make use of a two-step procedure to generate 3-D fields;

1. Specify 3-D fields from observations (for method ii) or CTMs (for method iii).

2. 'Adjust' these fields according to ensure that they are consistent with observed values at the background site of Mace Head

Ozone boundary conditions for UNI-ACID are simply taken from pre-calculations done with the more complex UNI-OZONE model.

6.1.1 Global datasets for Ozone:

Several datasets are available which can be used to specify background ozone levels. These include 2-D or 3-D climatological datasets (Logan 1998, Fortuin and Kelder 1998) derived from ozonesonde data, and 3-D datasets from global or hemispheric models (e.g UiO, TM3). The default set is derived from the climatological O_3 data published by Logan (1998). Logan use sonde data in combination with surface and satellite data to derive gridded O_3 data of 4° latitude by 5° longitude for 13 pressure levels.

The climatological data sets have the advantage that they are based upon actual measurements, although it should be admitted that the limited number of ozonesondes leads to crude spatial averaging. Both the Logan and Fortuin datasets underestimate ozone concentrations seen at sites on Europe's western coastline. The model-derived datasets have greater spatial resolution, can be obtained for a number of years, including far-future scenarios. However, these large-scale models still have problems reproducing observations within the accuracy needed for input to EMEP-scale calculations.

6.1.2 The 'Mace-Head' adjustment

In order to overcome the limitations of the above data-sets, and also to take into account year-to-year variations in the background ozone, we have devised a methodology which is heavily based upon a study of observations made at the site Mace Head on the west coast of Ireland. This site is ideally suited as a background site for mid-latitude air masses, and has been in operation for many years. Derwent et al. (1998) analysed observed ozone concentrations at this site with respect to the origin of their air masses. Three different techniques (including sector-analysis) were used to attribute concentrations to either the Northern Hemispheric Background, or to air masses influenced by European sources. All techniques produced remarkably similar results, suggesting that all 3 techniques were valuable for identifying clean air masses. The study also found that concentrations of O_3 (and CO) were basically uniform in a wide sector for air masses arriving from Iceland to Barbados - in other words, it confirmed the view of a general well-mixed background air mass.

For the EMEP model we have made use of an extended version of this analysis. Ozone concentrations from Mace Head have been sorted using sector-analysis, ob-

tained using trajectories obtained from `http://www.emep.int` [1] . Monthly mean values of the ozone associated with easterly sectors (sectors 6-8) have been calculated. Where fewer than 15 days were available to make an average for a particular year, averages from a full 10-year analysis were substituted for the missing days.

In order to generate an adjustment factor, the monthly values of observed O_3 derived using this procedure, denoted O_3^{MH}, are compared with the average surface concentrations from the global datasets in the south-west quadrant of the EMEP domain, denoted O_3^{GD}. (Thus, if the coordinates of Mace Head are denoted x_M, y_M, O_3^{GD} is the average concentration from model domain $x = 1..x_M$, $y = 1..y_M$). If the difference between the two datasets obtained in this way is Δ (=O_3^{MH}-O_3^{GD}, in ppb), we simply add Δ to the ozone boundary conditions over the whole domain. Since the concentrations of ozone are generally increasing with height in the model domain (from say 40 ppb to several hundred ppb), then the effect of this constant Δ term is greatest for the surface layer and quite small at say 5-10 km height.

Although simple, this procedure ensures that the BCs used for ozone are realistic in the mid-latitude region near ground level. Although based entirely upon one station, this correction has been found to result in good BCs for almost all sites on the west coast of Europe, ranging from Norway to Spain (Simpson et al. 2003a).

6.2 Prescribed values

In method (iv), simple functions have been chosen, designed to enable concentration values that correspond to observations. The concentrations are adjusted in the vertical and for latitude and time of the year (monthly fields) to match the observed distributions.

The annual cycle of each species is represented with a cosine-curve, using the annual mean near-surface concentration, C_0, the amplitude of the cycle ΔC, and the day of the year at which the maximum value occurs, d_{max}. Table 6.2 lists these parameters.

We first calculate the seasonal changes in ground-level BC concentration, C_0, through:

$$C_0 = C_{mean} + \Delta C \cdot \cos\left(2\pi \frac{(d_{mm} - d_{\mathrm{max}})}{n_y}\right) \tag{6.1}$$

where n_y is the number of days per year, d_{mm} is the day number of mid-month (assumed to be the 15th), and d_{max} is day number at which C_0 maximises, as given in Table 6.2. Changes in the vertical are specified with a scale-height, H_z, also given in Table 6.2:

$$C_i(h) = C_0 \exp(-h/H_z) \tag{6.2}$$

[1] Prior to 1996, sectors from Valentia had to be used. However, results calculated after 1996 show almost identical sector-results, regardless of the choice of Mace Head or Valentia

Table 6.2: Parameters used to set prescribed boundary conditions

	C_{mean} ppb	d_{max} days	ΔC ppb	H_z km	C^v_{min} ppb	C^h_{min} ppb
SO2	0.15	15.0	0.05	∞	0.15	0.03
SO4	0.15	180.0	0.00	1.6	0.05	0.03
NO	0.1	15.0	0.03	4.0	0.03	0.02
NO2	0.1	15.0	0.03	4.0	0.05	0.04
PAN	0.20	120.0	0.15	∞	0.20	0.1
HNO3	0.1	15.0	0.03	∞	0.05	0.05
CO	125.0	75.0	35.0	25.0	70.0	30.0
C2H6	2.0	75.0	1.0	10.0	0.05	0.05
C4H10	2.0	45.0	1.0	6.0	0.05	0.05
HCHO	0.7	180.0	0.3	6.0	0.05	0.05
CH3CHO	2.0	180.0	0.5	6.0	0.05	0.05

Notes: See text for definition of terms. Concentrations and other parameters estimated largely from Warneck (1988), Derwent et al. (1998), Ehhalt et al. (1991), Emmons et al. (2000), Isaksen and Hov (1987), Penkett et al. (1993), Solberg et al. (1996, 2000) and University of Oslo CTM2 model (Sundet 1997).

Table 6.3: Latitude factors applied to prescribed boundary and initial conditions.

Component	Latitude (°N)								
	30	35	40	45	50	55	60	65	70-90
SO2[a]	0.05	0.15	0.3	0.8	1.0	0.6	0.2	0.12	0.05
HNO3[b]	1.00	1.00	1.00	0.85	0.7	0.55	0.4	0.3	0.2
PAN	0.15	0.33	0.5	0.8	1.0	0.75	0.5	0.3	0.1
CO	0.6	0.7	0.8	0.9	1.0	1.0	0.95	0.85	0.8

Notes: (a) Applied also for SO_4, NO, NO_2; (b) Applied also for HCHO, CH_3CHO; See Simpson (1992) for sources of data

where $C_i(h)$ is the concentration at height h (in km). For simplicity we set h to be the height of the centre of each model layer assuming a standard atmosphere. Values of C_i are constrained to be greater or equal to the minimun values, C^v_{min}, given in Table 6.2. For some species a latitude factor, given in Table 6.3, is also applied. Values of C_i adjusted in this manner are constrained to be greater or equal to the minimun values, C^h_{min}, given in Table 6.2.

Finally for UNI-OZONE, we simply specify constant mixing ratios over the whole model domain, valid for 1990 (see section 6.3 for other years), for two species. These

Table 6.4: Prescribed concentrations of OH and CH_3COO_2 in UNI-ACID, as function of time-of-day and solar zenith angle (θ).

Compound	Night	Day
OH	10^4	$10^4 + 4 \cdot 10^6 \; e^{(-0.25/cos\theta)}$
CH_3COO_2	10^6	$5 \cdot 10^5 + 2.5 \cdot 10^6 \; e^{(-0.25/cos\theta)}$

Notes: Units: molecules cm^{-3}. Values below clouds are reduced with a factor of 0.5 times the fractional cloud cover.

are CH_4 1780 ppb; H_2 600 ppb

In UNI-ACID concentrations of OH and CH_3COO_2 are prescribed by simple functions of the solar zenith angle, θ, as described in table 6.4. Values below clouds are reduced with a factor of 0.5 times the fractional cloud cover.

6.3 Trends in boundary conditions

The BC values discussed above are assumed appropriate for the year 1990. For other years these values are adjusted using trend factors. These trend factors are summarised in Table 6.5.

Table 6.5: Assumed trends for boundary concentrations

Species	Trend , pre-1990 %/year	Trend , post-1990 %/year	Notes
O3	1	(a)	(b)
CO	0.85	0	(c)
VOC	0.85	0	(d)
CH4	0.91	0.2	(e)

Notes: (a) Mace-head correction applied on yearly basis to climatological values from 1990-current year, see section 6.1.2. (b) pre-1990 from Janach (1989), Low et al. (1990), Volz and Kley (1988), Bojkov (1986), Logan (1994) (c) Trend for CO of 0.85%/yr from Zander et al. (1989b); (d) Trend for ethane of 0.85%/yr from Ehhalt et al. (1991). Same trends assumed for n-butane and ethene. (e) Pre-1990 values from Zander et al. (1989a) for 1975-1990. Post-1990 values valid for 1990-2000, derived from Mace-Head observations.

CHAPTER 7

Chemistry

This chapter details the chemical schemes of both the UNI-OZONE and UNI-ACID versions of the model. In fact, the UNI-ACID chemistry is almost a pure subset of UNI-OZONE, since the latter now includes ammonium chemistry, gas and aqueous oxidation of SO_2 to sulphate, providing a comprehensive chemistry for both photo-oxidant and acidifi cation studies.

7.1 Species used

Table 7.1 list the chemical compounds used in the model, and Table 7.2 gives more description where required. Most species are suffi ciently long lived that they are included in both the advection and chemical equations. The species labelled "short-lived" have suffi ciently short lifetimes that their concentrations are essentially controlled by local chemistry, so they are not included among the advected species.

Note that this list excludes a number of intermediate species which are assumed to react immediately upon formation. For example, H atoms react immediately with O_2 to form HO_2, and so are not included explicitly.

7.2 Photo-dissociation rates

Table 7.3 lists the photolysis reactions used in the model. The reactions are taken from Simpson et al. (1993), with minor updates. The calculation of photodissociation rates (J-values) is identical to the methodology used for the earlier EMEP oxidant model (Jonson et al. 2001). J-values are calculated for clear sky conditions and for two predefi ned clouds using the phodis routine (Kylling et al. 1998). Ozone concentrations

Table 7.1: Calculated species in the EMEP MSC-W checmical scheme. Species given are for UNI-OZONE. Species in bold font are also included in UNI-ACID

Advected species				
O3	**NO**	**NO2**	**PAN**	MPAN
NO3	N2O5	ISONO3	**HNO3**	CH2CCH3
CH3COO2	MACR	ISNI	ISNIR	GLYOX
MGLYOX	MAL	MEK	MVK	HCHO
CH3CHO	C2H6	NC4H10	C2H4	C3H6
OXYL	ISOP	CH3O2H	C2H5OOH	secC4H9O2H
ETRO2H	PRRO2H	OXYO2H	MEKO2H	MALO2H
MVKO2H	MARO2H	ISRO2H	H2O2	CH3COO2H
MAR2O2H	ISONO3H	ISNIRH	CH3OH	C2H5OH
H2	CO	CH4	**SO2**	**SO4**
pNO3	**NH3**	**AMSU**	**AMNI**	**PM2.5**
PMco				
Short-lived:				
OD	OP	OH	HO2	CH3O2
C2H5O2	SECC4H9O2	ISRO2	ETRO2	PRRO2
OXYO2	MEKO2	MALO2	MVKO2	MACRO2

from a 2-D global model, extending from the surface to 50 km (Stordal et al. 1985) are scaled by observed total ozone columns from Dutsch (1974). Cloud base for both the predefined clouds is at 1 km above the ground. The first predefined cloud is 3 km deep, with a water content of 0.7 g cm^{-3} and a mean droplet radius of 10 μm. The second predefined cloud is 1 km deep, with water content of only 0.3 g cm^{-3} and a mean droplet radius of 10 μm. The J-values are calculated using the new recommendations for absorption cross sections and quantum yields from DeMore et al. (1997). For UNI-ACID, only the photolysis of NO_2 is included.

7.3 Chemical Mechanism

Table 7.5 gives a complete listing of the chemical mechanism used in the photo-oxidant model. Rate-coefficients for some 3-body reactions are given in Table 7.4. This scheme is based up the ozone chemistry from the Lagrangian photo-oxidant model (Simpson et al. 1993, Simpson 1995, Andersson-Sköld and Simpson 1999, Kuhn et al. 1998), but with additional reactions introduced to extend the model's coverage to acidification and eutrophication issues. These additions include ammonium chemistry, gas and aqueous oxidation of SO_2 to sulphate, and night-time production of nitrate. Additionally, a coarse particle nitrate species has been introduced. Rate-constants have been updated and in some cases replaced by Troe expressions (Table 7.4) to allow their application to the greater range of temperatures and pressures inherent in the 3-D

Table 7.2: Abbreviations used for some chemical species

SO4, pNO3	Particulate sulphate (fine-mode), nitrate (coarse mode)
AMSU, AMNI	$(NH_4)_{1.5}SO_4$, NH_4NO_3
PM2.5, PMco	fine particles ($d < 2.5\mu m$), course-mode particles ($2.5\mu m < d < 10\mu m$)
OXYL, ISOP	o-xylene, C5H10 (isoprene)
PAN, MPAN	$CH_3COO_2NO_2$, $CH_2CH(CH_3)COO_2NO_2$ (from isoprene chemistry)
GLYOX, MGLYOX	HCOHCO, CH3COCHO
MAL	CH3COCH=CHCHO
MEK	$CH_3COC_2H_5$ (methyl-ethyl-ketone
MVK	CH3C(=O)CH=CH2 (methyl-vinyl-ketone)
MACR	CH_2CCH_3CHO (methacrolein)
ISNI	isoprene-nitrate
peroxy radicals	
$ETRO2$, $PRRO2$, $secC4H9O2$, $ISRO2$, $OXYO2$, $MEKO2$, $MALO2$, $MVKO2$, $MACRO2$, $CH2CCH3$, $ISNIR$, $ISONO3$	From ethene, propene, n-butane, isoprene (6-isomers), o-xylene, MEK, MAL, MVK, ISNI, MACR, and CH2CCH3. ISONO3 is an isoprene-NO3 adduct.
Hydro-peroxy radicals	
$ETRO2H$, $PRRO2H$, $secC4H9O2H$, $ISRO2H$, $OXYO2H$, $MEKO2H$, $MALO2H$, $MVKO2H$, $MARO2H$, $MAR2O2H$, $ISNIRH$, $ISONO3H$	From ETRO2, PRRO2, secC4H9O2, ISRO2, OXYO2, MEKO2, MALO2, MVKO2, MACRO2, CH2CCH3, ISNIR and ISONO3

model domain.

Full details of the sources and methodology behind the basic photo-oxidant reaction schemes are given in Simpson et al. (1993) and Simpson (1995). Reaction coefficients are largely from DeMore et al. (1997), Atkinson et al. (1996, 1992), Atkinson (1990).

Sections 7.4-7.6 below detail the reactions forming sulphates, nitrates and ammonium compounds, which builds upon on those of (Hov et al. 1988, Iversen 1990, Berge and Jakobsen 1998).

Table 7.3: Photolysis Reactions, units of s^{-1}

O3	→	O3P + O2
O3	→	O1D + O2
NO2	→	NO + O3P
H2O2	→	OH + OH
HNO3	→	NO2 + OH
HCHO	→	HO2 + HO2 + CO
HCHO	→	CO + H2
CH3CHO	→	{CH3} + {HCO}
MEK	→	CH3COO2 + C2H5O2
GLYOX	→	1.9 CO + 0.5 HO2 + 0.1 HCHO
MGLYOX	→	CH3COO2 + CO + HO2
NO3	→	NO2 + O3P
N2O5	→	NO2 + NO3
CH3OOH	→	{CH3O} + OH
C2H5OOH	→	{C2H5O} + OH
CH3COO2H	→	CH3O2 + CO2 + OH
MEKO2H	→	CH3CHO+CH3COO2+OH
secC4H9O2H	→	OH + {secC4H9O}
ETRO2H	→	HO2 + OH + 1.56 HCHO + 0.22 CH3CHO
PRRO2H	→	CH3CHO + HCHO + HO2
OXYO2H	→	OH + MGLYOX + MAL + HO2
MALO2H	→	OH + HO2 + MGLYOX + GLYOX

Species in brackets {} are extremely short-lived. See Table 7.5 for products formed instantaneously from these. Rates for all organic hydroperoxides set equal to those of CH3O2H.

7.4 Sulphate production

The parameterization outlined below is previously described in Jonson et al. (2000). In the model SO_2 is oxidized to sulphate both in the gas phase and in the aqueous phase. We always assume equilibrium between gas and aqueous phase. It should be noted that in case the clouds occupy only a fraction of the grid volume, the total concentration (gas + aqueous) of soluble components are assumed to be uniformly distributed in the grid volume. If the cloud evaporates, the total concentration is always equal to the gas phase concentration.

For both gas and aqueous phase reactions we scale the reaction rates, rather than the concentrations, by the solubility and cloud volume fractions. In the present calculations we have assumed a constant pH value of 4.5 and cloud liquid water content of

0.6 g m^{-3} (inside the clouds).

In the parameterization of aqueous phase chemistry we assume that Henry's law is fulfilled:

$$[C_{(aq)}] = H_c P_c$$

where $[C_{(aq)}]$ is the concentration of any soluble gas C (mol l^{-1}) in the aqueous phase, H_c its Henry's law coefficient and P_c the partial pressure of C in the gas phase. In the aqueous phase many soluble gases undergo rapid reversible reactions such as acid-base equilibrium reactions. For these gases it is convenient to define an efficient Henry's law coefficient where the total amount of dissolved gases is taken into account. For example, the total amount of dissolved sulphur in solution (S(IV)) is equal to

$$[S(IV)_{(aq)}] = [SO_{2(aq)}] + [HSO^-_{3(aq)}] + [SO^{2-}_{3(aq)}]$$

The total dissolved S(IV) can be related to the partial pressure of SO_2 over the solution (P_{SO_2}) by

$$[S(IV)_{(aq)}] = H_{SO_2} P_{SO_2} \left(1 + \frac{K_1}{[H^+]} + \frac{K_1 K_2}{[H^+]^2}\right) \tag{7.1}$$

where H_{SO_2} is the Henry's law coefficient for SO_2 and K_1 and K_2 are the first and second ionisation constants for sulfurous acid. For pH values encountered in the atmosphere, the concentration of SO_3^{2-} is negligible and may be omitted, thus we can neglect the last term within the brackets in equation [7.1].

We define the effective Henry's law coefficient for SO_2 as:

$$H^* = [S(IV)_{(aq)}]/P_{SO_2}$$

and make use of the ideal gas law ($P_c = [C_{(g)}] \cdot RT$, where $[C_{(g)}]$ is gas phase concentration of C, R is the universal gas constant and T is temperature) in order to find an expression for the total concentration $[C_T]$ (gas + aqueous-phase) in a cloud volume:

$$\begin{aligned} [C_T] &= [C_{(g)}]/\alpha + [C_{(aq)}] \\ &= [C_{(aq)}]\left(1 + \tfrac{1}{H^* RT\alpha}\right) \end{aligned} \tag{7.2}$$

where α is the volume fraction of cloud water. Both $[C_T]$ and $[C_{(g)}]$ are in units M (mol/l). The fraction of the total (gas + aqueous) mass remaining in the interstitial cloud air (f_g) and the fraction absorbed by the droplets (f_{aq}) can be calculated as:

$$f_{aq} = 1 - f_g = \frac{[C_{(aq)}]}{[C_T]} = \frac{1}{1 + (H^* RT\alpha)^{-1}} \tag{7.3}$$

7.4.1 Gas phase

In the gas phase SO_2 is oxidized by a chain of reactions initiated by the reaction with OH:

$$SO_2 + OH \longrightarrow .....H_2SO_4$$

with reaction rate k_{sg} as given in Table 7.5. Since some of the SO_2 in a grid square is dissolved in clouds, we define a pseudo reaction rate to allow for this. Using f_{aq} as defined above, then for a fractional cloud volume W, the fraction of SO_2 in the gas-phase is given by:

$$F_g = [1 - f_{aq}W], \tag{7.4}$$

The pseudo-rate coefficient for model reaction OH + SO2 $\rightarrow$ SO4 then becomes $F_g \times k_{sg}$ as given in Table 7.5.

In the model we use the local cloud fraction, defined in the meteorological input fields, as an approximate value for the fractional cloud volume. With the parameterisation above, SO_2 oxidized both in the cloud free parts of the grid box and in the interstitial cloud air.

7.4.2 Aqueous phase

Although a number of oxidants may contribute in the oxidation, only O_3, H_2O_2 and O_2 catalyzed by metal ions are considered here. The rate of production for sulphate in solution is expressed as:

$$d[SO_4^{2-}]/dt = k_{cl1}[H_2O_2][SO_2] + (k_{cl2}[H^+][O_3] + k_{cl3})([SO_2] + [HSO_3^-])$$

where the reaction rate for the oxidation by O_3 is $k_{cl2} = 1.810^4[H^+]^{-0.4}$mol^{-1}l (Möller 1980) and the reaction rate for the oxidation by H_2O_2 is $k_{cl1} = 8.310^5$ mol^{-1}l (Martin and Damschen 1981). For the oxidation by O_2 catalyzed by metal ions we assume a reaction rate of $3.3 \cdot 10^{-10}$ molecules cm^{-1}, corresponding to a lifetime of approximately 50 hours.

As for the gas phase production of sulphate described in the previous section, we define pseudo reaction rates, taking into account the solubility of SO_2, H_2O_2 and O_3 and the fractional cloud volume. The pseudo reaction rates then becomes:

$$k'_{cl1} = k_{cl1}\Gamma\frac{H_{SO_2}}{H^*_{SO_2}}f_{SO_2}f_H W \tag{7.5}$$

$$k'_{cl2} = k_{cl2}\Gamma f_{SO_2}f_{O_3}W \tag{7.6}$$

$$k'_{cl3} = k_{cl3}f_{SO_2}W \tag{7.7}$$

for the for oxidation by H_2O_2, O_3 and O_2, respectively. f_H and f_{O_3} are the fractional solubilities of H_2O_2 and O_3 and Γ is a conversion factor converting k'_{cl1} and k'_{cl2} to molecules^{-1} cm^3. H_{SO_2} is the Henry's law constant for SO_2 and $H^*_{SO_2}$ is the effective Henry's law constant for S(IV).

7.5 Ammonium sulphate and ammonium nitrate

In the model ammonium sulphate is formed instantaneously from NH_3 and SO4, only limited by the availability of the least abundant of the two species. In the atmosphere ammonium sulphate is present in two forms, $(NH_4)_2SO_4$ or NH_4SO_4. We assume equal concentrations of the two forms, giving the EMEP pseudo species $(NH_4)_{1.5}SO_4$.

Any excess NH_3 may then react with HNO_3, forming ammonium nitrate (NH_4NO_3) through an equilibrium reaction. As a first step in this calculation the equilibrium concentration of NH_3 is calculated:

$$NH_3eq = \frac{NH_3 + HNO_3}{2} + \sqrt{\frac{(NH_3 - HNO_3)^2}{4} + k_{eq}}, \tag{7.8}$$

Where k_{eq} is the equilibrium constant defined below. The equilibrium concentration of NH_4HNO_3 (ammonium nitrate) is derived from NH_3:

$$NH_4NO_3eq = NH_4NO_3 + (NH_3 - NH_3eq) \tag{7.9}$$

Provided the difference between the equilibrium concentration and the former concentration is smaller than the former concentration, the equilibrium concentration becomes the new concentration of ammonium nitrate. Nitric acid (HNO_3) is adjusted accordingly, maintaining mass balance.

The equilibrium constant k_{eq} is calculated as recommended by Mozurkewich (1993). Below the point of deliquescence the equilibrium constant, now denoted K_p is given by the equation:

$$lnK_p = 118.87 + \frac{24084}{T} - 6.025ln(T) \tag{7.10}$$

where T is the temperature in Kelvin. Above the point of deliquescence the equilibrium constant, now denoted K_{aq} is given by:

$$K_{aq} = [P_1 - P_2(1 - \frac{RH}{100}) + P_3(1 - \frac{RH}{100})^2](1 - \frac{RH}{100})^{1.75}K_p \tag{7.11}$$

where both K_p and K_{aq} are in units of (molecules cm^{-3})^2. RH is the relative humidity in percent and P_1, P_2 and P_3 are given as:

$$lnP_1 = -135.94 + \frac{8763}{T} + 19.12ln(T)$$

$$lnP_2 = -122.65 + \frac{9969}{T} + 16.22ln(T)$$

$$lnP_3 = -182.61 + \frac{13875}{T} + 2446ln(T)$$

and the point of deliquescence is given as:

$$ln(RH_d/100) = \frac{618.3}{T} - 2.551$$

7.6 Nitrate production

Coarse nitrate

Coarse nitrate (pNO3) formation is assumed to take place at a rate k_{RH} (in s^{-1}) which depends on relative humidity (Eliassen et al. 1982):

$$\begin{aligned} k_{RH} &= 1.0 \times 10^{-4} \quad \text{for RH>90\%} \\ k_{RH} &= 5.0 \times 10^{-6} \quad \text{for RH<90\%} \end{aligned} \tag{7.12}$$

Night time production of HNO3 and nitrate

The night time production of total nitrate (defined as the sum of HNO_3 in the gas phase and NO_3 and ammonium nitrate in particulate form) is initiated by the gas phase reaction:

$$NO_2 + O_3 \longrightarrow NO_3 + O_2$$

N_2O_5 is formed in equilibrium with NO_3:

$$NO_3 + NO_2 \rightleftharpoons N_2O_5$$

N_2O_5 may further react with water on deliquescent aerosols, producing two NO_3^- molecules:

$$N_2O_5 + H_2O \longrightarrow 2NO_3^- + H^+$$

NO_3^- formed in the reaction above is assumed to evaporate. The HNO_3 thus formed will take part in the formation of ammonium nitrate as described in section 7.5 or coarse nitrogen as described above.

In daylight NO_3 is rapidly photolysed (Table 7.3) so that total nitrate is only produced through this path in the absence of sunlight. In winter, with low OH concentrations and many hours of darkness, the above reactions are believed to be the major source of total nitrate in the atmosphere (Dentener and Crutzen 1993). As noted above, the rate limiting step for the overall night time production of total nitrate is the initial reaction between NO_2 and O_3. However, at low humidities and/or low aerosol burden,

Table 7.4: Rate-constants for 3-body reactions. The reaction rates are calculated as: $k = \frac{K_0}{1+K_0/K_\infty} F^{(1+(log_{10}K_0/K_\infty)^2)^{-1}}$ The reaction numbers refers to the numbering in table 7.5.

	K_0	K_∞	F	
IN4	O + NO → NO_2	1.0E-31(300/T)$^{1.6}$[M]	3.0E-11(300/T)$^{-0.3}$	0.85
IN14	OH+NO_2 → HNO_3	2.6E-30(300/T)$^{2.9}$[M]	6.7E-11(300/T)$^{0.6}$	0.43
IN13	NO_2 + NO_3 → N_2O_5	2.7E-30(300/T)$^{3.4}$[M]	2.0E-12(300/T)$^{-0.2}$	0.33
IN15	N_2O_5 → NO_2 + NO_3 × e$^{(-11000/T)}$[M]	1.0E-3e(300/T)$^{3.5}$ × e$^{(-11080/T)}$	9.7E+14(300/T)$^{-0.1}$	0.33
EE1	OH + C_2H_4 → $CH_2O_2CH_2OH$	7.0E-29(300/T)$^{3.1}$[M]	9.0E-12	0.7
RR2	OH + C_3H_6 → $CH_3CHO_2CH_2OH$	8.0E-17(300/T)$^{3.5}$[M]	3.0E-11	0.5
EA7	CH_3COO_2 + NO_2 → PAN	2.7E-28(300/T)$^{7.1}$[M]	1.2E-11(300/T)$^{0.1}$	0.3
EA8	PAN + → CH_3COO_2 + NO_2	4.9E-3e$^{(-12100/T)}$[M]	5.4E+16e$^{(-13830/T)}$	0.3

the overall reaction can be limited by the availability of aerosols. The parameterization of this process is a simplification of the parameterization suggested by Dentener and Crutzen (1993). In the calculations we assume that the availability deliquescent aerosols is proportional to the sulphate concentration, represented as a volume fraction V of sulphate aerosols:

$$V = \frac{S \times M_s}{A_0 \rho}$$

where S is the concentration of sulphate (molecules cm^{-3}), M_s is the molecular weight of sulphate, A_0 is Avogadros number and ρ is the aerosol density (g cm^{-3}). An expression for the conversion of N_2O_5 to NO_3^- on deliquescent aerosols is expressed as:

$$K_a = V \frac{3\alpha v}{4r} RH/100. \tag{7.13}$$

where α is the sticking coefficient (10^{-2}), v is the mean molecular speed for the N_2O_5 molecules and r is the average radius of the aerosols (0.3 μ m).

UNI-ACID version

In the UNI-ACID version some of the above equations are slightly modified as OH, CH_3COO_2, H_2O_2 and O_3 concentrations are not calculated in the model. This is discussed in section 6.2. As NO_3 and N_2O_5 are not included in the UNI-ACID version we take advantage of the fact that the reaction forming NO_3 (IN7) is assumed to be the rate limiting step and combine this reaction with the subsequent reaction steps:

$$2NO_2 + O_3 + H_2O \longrightarrow 2NO_3^- + 2H^+ + O_2$$

This overall reaction is limited by the aerosol burden in much the same way as the NO_3^- production in the UNI-OZONE model version.

7.7 Secondary organic aerosol and other chemistries

The implementation of chemical schemes in the unified model is now done using a pre-processor written in Perl. Thus, whilst the UNI-ACID and UNI-OZONE labels are convenient for describing two 'standard' chemistries within the modelling system, the new unified model can be quickly switched to accommodate new reactions and species.

As a relevant example, the unified model can also be run with the secondary organic aerosol (SOA) formation scheme which is described in detail in Andersson-Sköld and Simpson (2001). Three different mechanism for treating the formation of SOA were investigated, with biogenic terpenes as a main source. However, an important conclusion of Andersson-Sköld and Simpson was that such SOA schemes are not yet reliable enough for use in policy-related modelling, largely because the fundamental scientific understanding of SOA is at such an early stage. Thus, SOA modelling is regarded as a research activity within EMEP and this mechanism is not included in the standard model.

7.8 Numerical solution

The chemical equations are solved using the TWOSTEP algorithm tested by Verwer and Simpson (1995). At present, with an advection time-step dt_{advec} of 20 minutes (1200 s) the algorithm starts with five successive timesteps of dt_{chem}=20 seconds followed by seven larger timesteps of dt_{chem}=1100/7=157 s. Compared with a fixed timestep, increasing timesteps has been found more efficient, since at the start of the process the system is further away from a steady-state situation. This scheme improves with iteration. In the 4 layers near the ground, where emission and often reaction tendencies are highest, we perform 3 iterations each timestep. Above this, 2 iterations are performed, except for the uppermost 6 layers where 1 iteration is believed sufficient.

Table 7.5: Photo-oxidant Chemistry of the Unified model. Full UNI-OZONE chemistry given, with UNI-ACID reactions listed in **bold face**

Code	Rate coefficient	Reaction
		Inorganic chemistry
IN1	6.0E-34*(t/300.0)$^{-2.3}$	O+O2+M → O3
IN2	1.8E-11*exp(107.0/t)	OD+N2 → O
IN3	3.2E-11*exp(67.0/t)	OD+O2 → O
IN4	Troe	O+NO+M → NO2
IN5	2.2E-10	OD+H2O → OH+OH
F	Immediate	H+O2 → HO2
IN6	**1.8E-12*exp(-1370./t)**	**O3+NO → NO2**
IN7	**1.2E-13*exp(-2450./t)**	**O3+NO2 → NO3**
IN8	1.9E-12*exp(-1000./t)	O3+OH → HO2
IN9	1.4E-14*exp(-600./t)	O3+HO2 → OH
IN10	1.8E-11*exp(110./t)	NO+NO3 → NO2+NO2
IN11	3.7E-12*exp(240./t)	NO+HO2 → NO2+OH
IN12	7.2E-14*exp(-1414./t)	NO2+NO3 → NO+NO2
IN13	Troe	NO2+NO3 → N2O5
IN14	**Troe**	**NO2+OH → HNO3**
IN15	Troe	N2O5 → NO2+NO3
IN16	4.8E-11*exp(250./t)	OH+HO2 → H2O
IN17	2.9E-12*exp(-160./t)	OH+H2O2 → HO2
IN18	7.7E-12*exp(-2100./t)	OH+H2 → H
IN19	1.05E-14*exp(785./t)	OH+HNO3 → NO3
IN20	FHO2*2.3E-13*exp(600./t)	HO2+HO2 → H2O2
IN21	FHO2*M*1.7E-33*exp(1000./t)	HO2+HO2 → H2O2
		Sulphur and Ammonium chemistry
SA1	**2.0**$\times 10^{-12}.F_g$ **(sec.7.4.1)**	**OH + SO2 → HO2 + SO4**
SA2	**k'**$_{cl1}$**, sec. 7.4.2**	**SO2 + H2O2 → SO4**
SA3	**k'**$_{cl2}$**, sec. 7.4.2**	**SO2 + O3 → SO4**
SA4	**k'**$_{cl3}$**, sec. 7.4.2**	**SO2 (+ Fe) → SO4**
F	**Immediate**	**SO4 + NH3 → AMSU**
SA5	**Sec.7.5**	**NH3 + HNO3 ⇌ AMNI**
		Methane chemistry

continued on next page

	Rate coeffi cient	Reaction
ME1	$3.9E-12*exp(-1765./t)$	OH+CH4 → CH3
F	Immediate	CH3+O2 → CH3O2
ME2	K_{RO2NO}	CH3O2+NO → CH3O+NO2
ME3	5.9E-14*exp(509./t)	CH3O2+CH3O2→CH3O+CH3O
ME4	7.04E-14*exp(365./t)	CH3O2+CH3O2→CH3OH+HCHO
ME5	3.1E-12*exp(-360./t)	OH+CH3OH→HO2+HCHO
ME6	3.8E-13*exp(780./t)	HO2+CH3O2 → CH3O2H
F	Immediate	CH3O+O2 → HCHO+HO2
ME7	8.6E-12*exp(20./t)	OH+HCHO → HCO
F	Immediate	HCO+O2 → CO+HO2
ME8	K_{H1}	CH3O2H + OH → HCHO + OH
ME9	K_{H2}	CH3O2H + OH → CH3O2
ME10	5.8E-16	NO3+HCHO → HNO3+HCO
ME11	K_{PCO}	OH+CO → H
		Ethane chemistry
EA1	7.9E-12*exp(-1030./t)	OH+C2H6 → C2H5O2
EA2	8.7E-12	C2H5O2+NO → C2H5O+NO2
EA3	2.7E-13*exp(1000./t)	C2H5O2+HO2 → C2H5OOH
EA4	K_{H3}	C2H5OOH+OH → CH3CHO+OH
EA5	K_{H2}	C2H5OOH+OH → C2H5O2
F	Immediate	C2H5O+O2 → HO2+CH3CHO
EA6	5.6E-12*exp(310./t)	OH+CH3CHO → CH3COO2
EA7	**Troe**	**CH3COO2+NO2 → PAN**
EA8	**Troe**	**PAN → CH3COO2+NO2**
EA9	2.0E-11	CH3COO2+NO → NO2+CH3
EA10	5.5E-12	CH3O2+CH3COO2 → CH3O+CH3
EA11	5.5E-12	CH3O2+CH3COO2 → CH3COOH+HCHO
EA12	2.8E-12*exp(530/t)	CH3COO2+CH3COO2 → CH3+CH3
EA13	1.3E-13*exp(1040./t)	CH3COO2+HO2 → CH3COO2H
EA14	1.9E-12*exp(190./t)	CH3COO2H+OH → CH3COO2
EA15	3.0E-13*exp(1040./t)	CH3COO2+HO2 → O3 + [CH3COOH]
		Ethanol chemistry
EO1	3.69E-12*exp(-70./t)	OH+C2H5OH → CH3CHO + HO2
		n-butane chemistry
BU1	1.64E-11*exp(-559./t)	OH+NC4H10 → SECC4H9O2
BU2	K_{RO2NO}	NO+SECC4H9O2→NO2+SECC4H9O

continued on next page

	Rate coeffi cient	Reaction
F	Immediate	SECC4H9O→ 0.65 HO2 + 0.65 CH3COC2H5 + 0.35 CH3CHO +0.35 C2H5O2
BU3	1.15E-12	OH+CH3COC2H5 → CH3COCHO2CH3
BU4	K_{RO2NO}	CH3COCHO2CH3+NO→ NO2+CH3COO2+CH3CHO
BU5	K_{HO2RO2}	CH3COCHO2CH3+HO2→ CH3COCHO2HCH3
BU6	4.8E-12	CH3COCHO2HCH3+OH→ CH3COCHO2CH3
BU7	K_{HO2RO2}	SECC4H9O2+HO2→ SECC4H9O2H
BU8	K_{H2}	SECC4H9O2H+OH→ SECC4H9O2
BU9	K_{H3}	SECC4H9O2H+OH→ OH+CH3COC2H5
		Ethene chemistry
EE1	Troe	C2H4+OH → CH2O2CH2OH
EE2	K_{RO2NO}	CH2O2CH2OH+NO→NO2+HCHO+HCHO+HO2
EE3	K_{HO2RO2}	CH2O2CH2OH+HO2 → CH2OOHCH2OH
EE4	K_{H3}	CH2OOHCH2OH+OH → CH3CHO + OH
EE5	K_{H2}	CH2OOHCH2OH+OH → CH2O2CH2OH
EE6	1.2E-14*exp(-2630./t)	C2H4+O3→HCHO+0.44 CO+ 0.12 HO2+ 0.4 HCOOH+ 0.13 H2
		Propene chemistry
PR1	6.5E-15*exp(-1880./t)	O3+C3H6→ 0.5 HCHO+ 0.5 CH3CHO+ 0.07 CH4+ 0.4 CO+ 0.28 HO2+ 0.15 OH+ 0.31 CH3O2+ 0.07 H2
PR2	Troe	OH+C3H6 → CH3CHO2CH2OH
PR3	K_{RO2NO}	NO+CH3CHO2CH2OH→NO2+CH3CHO+HCHO+HO2
PR4	K_{HO2RO2}	CH3CHO2CH2OH+HO2→CH3CHOOHCH2OH
PR5	K_{H3}	CH3CHOOHCH2OH+OH→ CH3COC2H5+OH
PR6	K_{H2}	CH3CHOOHCH2OH+OH→ CH3CHO2CH2OH
		o-xylene chemistry
XY1	1.37E-11	OXYL+OH→OXYO2
XY2	K_{RO2NO}	OXYO2+NO→NO2+MGLYOX+MAL+HO2
XY3	K_{HO2RO2}	OXYO2 + HO2→OXYO2H
XY4	1.7E-11	OXYO2H + OH → OXYO2
XY5	2.0E-11	MAL+OH→MALO2
XY6	K_{RO2NO}	MALO2+NO→NO2+HO2+MGLYOX+GLYOX
XY7	K_{HO2RO2}	MALO2+HO2→MALO2H
XY8	2.4E-11	MALO2H+OH → MALO2
XY9	1.1E-11	OH+GLYOX→HO2+CO+CO
XY10	1.70E-11	OH+MGLYOX→CH3COO2+CO

continued on next page

	Rate coeffi cient	Reaction
		Isoprene chemistry
IS1	12.3E-15*exp(-2013/t)	ISOP+O3→ 0.67 MACR, 0.26 MVK+0.3 O, 0.55 OH+0.07 C3H6+0.8 HCHO+0.06 HO2+0.05 CO
IS2	2.54E-11*exp(410./t)	ISOP+OH→ISRO2
IS3	K_{RO2NO}	ISRO2+NO→ 0.32 MACR+0.42 MVK+0.74 HCHO, 0.14 ISNI+0.12 ISRO2+0.78 HO2+0.86 NO2
IS4	4.13E-12*exp(452./t)	MVK+OH→MVKO2
IS5	K_{RO2NO}	MVKO2+NO→ 0.684 CH3CHO+0.684 CH3COO2+ 0.266 MGLYOX+0.266 HCHO+0.05 ISNI+0.95 NO2+0.95 HO2
IS6	K_{HO2RO2}	ISRO2+HO2→ISRO2H
IS7	2.0E-11	ISRO2H + OH→OH+ISRO2
IS8	8.0E-18	ISRO2H + O3→*0.7:HCHO
IS9	1.86E-11*exp(175./t)	MACR+OH→0.5 AOH1+ 0.5:MACRO2
IS10	1.0E-11	MACRO2+NO2→MPAN
IS11	1.34E+16*exp(-13330./t)	MPAN → MACRO2+NO2
IS12	2.0E-11	MACRO2+NO→CH2CCH3+NO2
IS13	K_{RO2NO}	CH2CCH3+NO →NO2+CH3COC2H5+HO2
IS14	4.32E-15*exp(-2016./t)	MVK+O3→0.82 MGLYOX+0.8 HCHO+0.2 O+ 0.05 CO+0.06 HO2+0.04 CH3CHO+0.08 OH
IS15	3.35E-11	ISNI+OH→ISNIR
IS16	K_{RO2NO}	ISNIR+NO→ 0.05 HO2+ 2.0 NO2+ 0.95 CH3CHO+ 0.95 CH3COC2H5
	(Isoprene-NO3 chemistry:)	
IN1	7.8E-13	ISOP +NO3→ISONO3
IN2	K_{RO2NO}	ISONO3+NO→1.1 NO2 + 0.8 HO2 + 0.85 ISNI + 0.1 MACR + 0.15 HCHO + 0.05 MVK
IN3	K_{HO2RO2}	MVKO2 + HO2 → MVKO2H
IN4	K_{HO2RO2}	MACRO2 + HO2 → MARO2H
IN5	K_{HO2RO2}	CH2CCH3+ HO2 → MAR2O2H
IN6	K_{HO2RO2}	ISNIR + HO2 → ISNIRH
IN7	K_{HO2RO2}	ISONO3 + HO2 → ISONO3H
IN8	3.2E-11	MAR2O2H + OH → CH2CCH3
IN9	2.0E-11	ISONO3H + OH → ISONO3
IN10	2.2E-11	MVKO2H + OH → MVKO2
IN11	3.7E-11	ISNIRH + OH → ISNIR
IN12	3.7E-11	MARO2H + OH → MACRO2
		Aerosol chemistry

continued on next page

	Rate coeffi cient	Reaction
AE1	1.0e-5	H2O2 $\rightarrow$ aerosol
AE2	1.0e-5	CH3O2H $\rightarrow$ aerosol
AE3	**Sec. 7.6**	**N2O5 $\rightarrow$ 2 x nitrate**
AE4	**RH dependent, Sec. 7.6**	**HNO3 $\rightarrow$ pNO3**

Notes:
"t" is temperature, M is third body.
Generic reaction rates:
FHO2=(1.+1.4E-21*H2O*exp(2200./t))
K_{RO2NO}=4.2E-12*exp(180./t)
K_{HO2RO2}=1.0E-11
K_{H1}=1.0E-12*exp(190./t)
K_{H2}=1.9E-12*exp(190./t)
K_{H3}=5.8*K_{H1}
K_{PCO}=$1.5 \times 10^{-13}(1.0 + 0.6P_{atm})$ where P_{atm} is air pressure in atmospheres.
Reactions IN3...IN12 were added since Note 2/93, see Simpson, 1995
Reaction coeffi cients are in units of s^{-1} for unimolecular reactions, cm^3 molecule^{-1} s^{-1} for bimolecular reactions, and cm^6 molecule^{-2} s^{-2} for termolecular reactions. Reaction steps labelled as "Immediate" are given for clarity only.

Notes on UNI-ACID:
H_2O_2 and O_3 pre-calculated by UNI-OZONE
Parameterization of OH and CH_3COO_2 described in section 6.2.

CHAPTER 8

Dry Deposition

8.1 Resistance formulation

Over a particular land-surface, the loss rate of a particular gas i to the surface, within a volume of unit area and height Δz, is given by the product of a deposition velocity at height z_{ref} and the concentration (C_i) at that height:

$$dC_i(z_{ref})/dt = -V_g(z_{ref}) \times C_i(z_{ref})/\Delta z \tag{8.1}$$

where

$$V_g = \frac{1}{R_a + R_b + R_c} \tag{8.2}$$

R_a (s m^{-1}) is the aerodynamic resistance between z_{ref} and the top of the vegetation canopy (formally, $d + z_0$, where d is the displacement height and z_0 the roughness length), R_b (s m^{-1}) is the quasi-laminar layer resistance to gas i, R_c (s m^{-1}) is the surface (canopy) resistance to gas i.

If we have several different land-use classes within a grid, the grid-average deposition rate is given by:

$$\widetilde{V_g} = \sum\nolimits_{k=1}^{N} f_k \times V_g^k \tag{8.3}$$

where $\widetilde{Q}$ symbolises throughout this text the grid-square average of any quantity Q, f_k is the fraction of land-use type k in the grid-square, and V_g^k is the deposition velocity for each land-use calculated with eqn [8.2].

Correction for rain-areas

In grids where rainfall occurs, we assume that the fraction of the surface which is wetted by precipitation is equal to the cloud area fraction a_{CL} (section 3.1). For soluble species (notably SO_2), deposition velocities are calculated assuming both dry and wet surfaces, i.e.:

$$V_{g,dry} = \frac{1}{R_a + R_b + R_{c,dry}}, \qquad V_{g,wet} = \frac{1}{R_a + R_b + R_{c,wet}} \tag{8.4}$$

With total deposition velocity obtained as simply $V_g = a_{CL}.V_{g,wet} + (1 - a_{CL}).V_{g,dry}$. It should be noted that even 'dry' deposition velocity rates are assumed to be affected by RH, see section 8.6.5.

Nitrogen dioxide

The exchange of nitrogen oxides at the surface is very difficult to parameterise in a good way, and observations often show emissions from the surface instead of deposition, especially at low NO_2 concentrations. In a crude attempt to reflect this, equation 8.1 is modified, based loosely upon observations presented in Walton et al. (1997), Fowler and Erisman (2003), Duyzer and Fowler (1994):

$$dC_{NO_2}(z_{ref})/dt = -V_g(z_{ref}) \times [C_{NO_2}(z_{ref}) - C_x]/\Delta z \tag{8.5}$$

where C_x is a threshold concentration, 4 ppb. Only deposition is allowed, so that there is no deposition of NO_2 with concentrations below 4 ppb.

8.2 Aerodynamic Resistance, R_a

The first steps in the derivation of sub-grid R_a are to derive a grid-square average Monin-Obukhov length, $\widetilde{L}$, similar to eqn. [3.1]:

$$\widetilde{L} = \frac{-\tilde{\rho}\, c_p\, \widetilde{T}_2\, \widetilde{u_*}^3}{k\, g\, \widetilde{H}} \tag{8.6}$$

The 3-D model meteorology includes wind-speed u for the centre of the lowest grid level, at around 45 m. We assume that this height is within or near the top of the surface layer, and proceed to calculate turbulence parameters based upon the *local* values of z_0 and d. These are simply derived from the height, h, of the vegetation (Table 5.1), using $d = 0.7h$, $z_0 = 0.1h$ (over water depends on u_*. We then estimate a new u_* based upon our z_{ref} wind. As a first estimate,we assume the local L is equal to the grid-cell $\widetilde{L}$. Then, :

$$u_* = \frac{u(z_{ref})\ k}{\ln\left(\frac{z_{ref}-d}{z_0}\right) - \Psi_m\left(\frac{z_{ref}-d}{L}\right) + \Psi_m\left(\frac{z_0}{L}\right)} \tag{8.7}$$

Ψ_m is the similarity function for momentum (eqn [3.3]). Having calculated u_* in this way, a better estimate of L can be found by substituting u_* in eqn [8.6]. The aerodynamic resistance for heat or scalars between any two levels z_2,z_1, is calculated with:

$$R_{a,h}(z_2, z_1) = \frac{1}{k \cdot u_*}\left[\ln\left(\frac{z_2-d}{z_1-d}\right) - \Psi_h\left(\frac{z_2-d}{L}\right) + \Psi_h\left(\frac{z_1-d}{L}\right)\right] \tag{8.8}$$

where Ψ_h is the similarity function for heat (eqn. [3.3]). For deposition calculations, we set z_2 to be the reference height z_{ref} and z_1 to be the top of quasi-laminar layer, $z_0 + d$, so that we use $Ra = Ra, h(z_{ref}, d + z_0)$.

8.3 Quasi-laminar layer resistance, R_b

$$R_b = \frac{2}{k.u_*}\left(\frac{Sc}{\mathrm{Pr}}\right)^{2/3} \tag{8.9}$$

Where Sc, the Schmidt number is equal to the ν/D_i, with ν being the kinetic viscosity of air (0.15 cm^2 s^{-1} at 20°C) and D_i is the molecular diffusivity of gas i, and Pr is the Prandtl number, 0.72. Over sea areas the expression of Hicks and Liss (1976) is used:

$$R_b = \frac{1}{k\ u_*} \cdot \ln\left(\frac{z_0}{D_i}\ ku_*\right) \tag{8.10}$$

8.4 Surface resistance, R_c

Surface (or canopy) resistance is the most complex variable in the deposition model, as it depends heavily on surface characteristics and the chemical characteristics of the depositing gas. Our approach makes use of bulk canopy resistances and conductances (R and G terms, where $G_x = 1/R_x$ for any x), and of unit-leaf-area (one-sided) resistances and conductances, which we denote with lower-case letters r, g. The general formula for bulk canopy conductances, G_c, is:

$$G_c = LAI \cdot g_{sto} + G_{ns} \tag{8.11}$$

where LAI is the leaf-area index (m^2 m^{-2}, one sided), g_{sto} is the stomatal conductance, and G_{ns} is the bulk non-stomatal conductance. For non-vegetative surfaces only the last term is relevant.

At sub-zero temperatures many of the following formulas use a low-temperature resistance. We use the formulation of Wesely (1989), where T_s is here in °C:

$$R_{low} = 1000\, e^{-(T_s+4)} \tag{8.12}$$

Nitric acid is a special case, since in normal conditions the surface resistance to HNO_3 is effectively zero. A minimum value of R_c of 1 s m^{-1} is enforced for numerical reasons, so for HNO_3 the whole canopy resistance is then simply given by:

$$R_c^{HNO_3} = \max(1.0, R_{low})$$

The more complex formulation for stomatal and non-stomatal conductances for other gases are dealt with below.

8.5 Stomatal conductance

Stomatal resistance is calculated with the multiplicative model of Emberson et al. (2000a):

$$g_{sto} = g_{max}\, f_{phen}\, f_{light}\, \max\{f_{min}, f_T\, f_{VPD}\, f_{SWP}\} \tag{8.13}$$

where g_{max} is the maximum stomatal conductance (m s^{-1}), and f_x are factors (from 0–1) accounting for time of year (leaf phenology), the minimum observed stomatal conductance (min), light (actually photon flux density, PFD), leaf-temperature (T), leaf-to-air vapour-pressure deficit (VPD), and soil-water potential (SWP). At the time of writing the current model version (rv1.8) does not include soil water, so effectively $f_{SWP} = 1$.

Table 8.1 lists g_{max} values (although here in mmole O_3 m^{-2} PLA s^{-1}, denoted g^m_{max}) along with values of other parameters needed for the conductance modelling. For pressure P and temperature T, g_{max} in m s^{-1} units is given by:

$$g_{max} = g^m_{max} RT/P \tag{8.14}$$

R is here the gas-constant (8.314 J/mole/K). At normal temperature and pressure, $g_{max} \approx g^m_{max}/41000$. For details of the functions used, and methods of calculating radiation in the canopy (for f_{light}) and VPD see Emberson et al. (2000a). Further discussion of this algorithm and evaluation can be found in Emberson et al. (2001, 2000a,b), Simpson et al. (2001, 2003b), Tuovinen et al. (2001).

Table 8.1: Land-scape specifi c parameters for stomatal conductance modelling

Land Class	g^m_{max} mmol O_3 m^{-2} PLA s^{-1}	f_{min}	Phenology			Light	Temperature			VPD		SWP	
			f_{phen_a}	f_{phen_b}	f_{phen_c}	α	T_{min} °C	T_{opt} °C	T_{max} °C	VPD_{max} kPa	VPD_{min} kPa	SWP_{max} MPa	SWP_{min} MPa
CF	160	0.1	0.2	130	130	0.0083	1	18	36	0.6	3.3	-0.76	-1.2
DF	134	0.13	0.3	50	50	0.006	6	20	34	0.93	3.4	-0.55	-1.3
NF	180	0.13	0.3	110	150	0.013	4	20	37	0.4	1.6	-0.4	-1
BF	200	0.03	0.3	110	150	0.009	4	20	37	1.8	2.8	-1.1	-2.8
TC	300	0.01	0.1	0	45	0.009	12	26	40	0.9	2.8	-0.3	-1.1
MC	156	0.019	0.1	0	45	0.0048	0	25	51	1.0	2.5	-0.11	-0.8
RC	360	0.02	0.2	20	45	0.0023	8	24	50	0.31	2.7	-0.44	-1.0
SNL	60	0.01	0.1	0	45	0.009	1	18	36	88.8	99.9	na	na
GR	270	0.01	1.0	0	0	0.009	12	26	40	1.3	3.0	-0.49	-1.5
MS	213	0.014	0.2	130	130	0.012	4	20	37	1.3	3.0	-1.1	-3.1

Notes: For defi nition of land-classes, see Table 5.1. For sources of data see Emberson et al. (2000a), except: DF: New values from UNECE (2003). Note that g_{age}, g_{light} and g_{temp} from Emberson et al. (2000a) have been renamed to f_{phen}, f_{light} and f_{temp} here, in order to distinguish these factors from true conductances. Conversion of g^m_{max} as given here to units of m s^{-1} is done using equation [8.14]. PLA = projected leaf area (m^2).

Table 8.2: Properties of gases for dry deposition calculations. Diffusivity ratio for a gas i, $D_r = D_{H2O}/D_i$, Effective Henry's coefficient, H^*, and Reactivity index $f0$. Based upon Wesely et al. (1985).

Gas	D_r	H^*	$f0$
SO2	1.9	1.0×10^{5}	0.0
O3	1.6	1.0×10^{-2}	1.0
NO2	1.6	1.0×10^{-2}	0.1
HNO3	1.9	1.0×10^{14}	0.0
H2O2	1.4	1.0×10^{5}	1.0
HCHO	1.3	6.0×10^{3}	0.0
CH3CHO[a]	1.6	15	0.0
OP[b]	1.6	2.4×10^{2}	0.1
NH3[c]	1.0	1.0×10^{5}	0.0
PAN	2.6	3.6	0.1

Notes: (a) Used for all aldehydes except HCHO; (b) OP=Wesely "Methyl hydroperoxide" - used for all hyroperoxides (c) H^* increased compared to Wesely value, reflecting European pH conditions.

Other gases

The methodology for stomatal conductance was been developed and tested originally for ozone, but stomatal conductance calculated for ozone is simply scaled for any other gas, i, using the ratio of the diffusivities in air of ozone and gas i. Table 8.2 gives the diffusivities (although expressed relative to water) used in the EMEP model.

8.6 Non-stomatal resistances

G_{ns} is calculated specifically for O_3, SO_2, and NH_3. Values for other gases are obtained by interpolation of the O_3 and SO_2 values (section 8.6.4). We will use superscripts to indicate the gas, with i for a general gas i.

8.6.1 Ammonia, $G_{ns}^{NH_3}$

The non-stomatal resistance R_{ns} for NH_3 is assumed to depend upon surface (2 m) temperature, T_s (°C), humidity levels, RH (%), and on the molar 'acidity ratio':

$$a_{SN} = 0.6 \times [SO_2]/[NH_3] \tag{8.15}$$

This acidity ratio is a first attempt to account for the observed changes in resistance in areas with different pollution climates (Erisman et al. 2001, Fowler and Erisman 2003). Other possible ratios include [NH_3+NH_4^+]/[SO_2 + SO_4^{2-}], but there is insufficient data upon which to chose between these ratios for modelling purposes at this time. The factor 0.6 is used to allow for the fact that the ratio of these gases at the surface should be higher than predicted by the EMEP model, due to the large vertical gradients of NH_3 above source areas.

The parameterisation of Smith et al. (2000) has been modified in order to take into account the effects of a_{SN}, based upon discussions with the Centre for Ecology and Hydrology (Smith et al. 2003). The resulting scheme can be expressed as:

$$\begin{array}{rcll} R_{ns} & = & \beta F_1(T_s, RH)\ F_2(a_{SN}) & (T_s > 0) \\ & & 200 & (-5 < T_s \leq 0) \\ & & 1000 & (T_s \leq -5) \end{array} \tag{8.16}$$

Where β is a normalising factor (0.0455), $F_1 = 10\log(T_s + 2)e^{((100-RH)/7)}$, and $F_2 = 10^{(-1.1099a_{SN}+1.6769)}$.

The F_1 term is identical to that of Smith et al. (2000) and provides a relationship of R_{ns} with temperature and relative humidity. The second function, F_2, is an equation derived from observations presented in Nemitz et al. (2001), and relates the value at 95% relative humidity and 10°C to the molar ratio of SO_2/NH_3. The two terms are equal for molar SO_2/NH_3 ratio 0.3. The factor β is introduced in order to normalize one equation to the other, i.e to ensure that the combined parameterisation is equal to the two separate terms for 95% relative humidity, 10°C and molar ratio 0.3.

For above-zero temperatures R_{ns} is constrained to lie between 10 and 200 s/m. Finally, we do not distinguish wet or dry surfaces in this formulation (they are included in the RH dependency used above), so the conductances are:

$$G_{ns,dry} = G_{ns,wet} = 1/R_{ns}$$

8.6.2 Ozone, $G_{ns}^{O_3}$

Our formulation of the non-stomatal conductance for ozone is more complicated than that of sulphur, but has been extensively evaluated (Emberson et al. 2000a, Tuovinen et al. 2001, 2003):

$$G_{ns}^{O_3} = SAI \cdot g_{ext} + \frac{1}{R_{inc} + R_{gs}^{O_3}} \tag{8.17}$$

where SAI is a surface area index ($m^2\ m^{-2}$) g_{ext} is the external leaf-resistance (cuticles+other surfaces), R_{inc} is the in-canopy resistance, and R_{gs} is the ground surface resistance (soil or other ground cover, e.g. moss).

Table 8.3: Base-Values of Ground-Surface Resistance for Sulphur Dioxide ($\hat{R}_{gs}^{SO_2}$) and Ozone ($\hat{R}_{gs}^{O_3}$). Units: s m^{-1}.

Landuse	$\hat{R}_{gs}^{SO_2}$	$\hat{R}_{gs}^{O_3}$
Forests, Mediterranean scrub	-	200
Crops	-	200
Moorland	-	400
Grasslands	-	1000
Wetlands	-	400
Tundra	500	400
Desert	1000	2000
Water	1	2000
Ice	100	2000
Urban	400	400

Notes: '-' - not used in formulation.

The external conductance g_{ext} is set at 1/2500 m s^{-1}. Base-values of R_{gs} (denoted $\hat{R}_{gs}$) are given in Table 8.3. These are modified for low temperature and snow cover (represented with $\delta_{snow} = 1$ when snow present, zero otherwise)[1] with:

$$R_{gs}^{O_3} = \hat{R}_{gs}^{O_3} + R_{low} + 2000\,\delta_{snow} \tag{8.18}$$

Following Erisman et al. (1994), the in-canopy resistance, R_{inc}, is defined as $b.SAI.h/u_*$, where h is the canopy height and $b = 14$ (s^{-1}) is an empirical constant. These paramaterisations and the choice of values are discussed in detail in Emberson et al. (2000a). We can note that much of the data concerning these deposition pathways is contradictory and much too inconclusive to enable a reliable treatment.

SAI is simply set to LAI+1 for forests, or LAI for non-crop vegetation. For crops a substantial part of the leaf area can be senescent. A simplified version of the methodology of Tuovinen et al. (2003), based upon the life-cycle of wheat, is applied:

$$\begin{aligned} SAI &= LAI + \left(\tfrac{5}{3.5} - 1\right) LAI \quad \text{for: } SGS < d_N < SGS + L_S \\ &= LAI + 1.5 \qquad\qquad\quad \text{for: } SGS + L_S < d_N < EGS \end{aligned} \tag{8.19}$$

Where d_N is the day number, and SGS, EGS, L_S are as defined in chapter 5. Outside the growing season, SAI = LAI = 0 m^2 m^{-2}.

[1]The EMEP model uses snow cover from monthly climatological tables, so this approach applies mainly to extensive snow and ice-covered areas

8.6.3 Sulphur Dioxide, $G_{ns}^{SO_2}$

The canopy conductance of SO_2 is strongly controlled by wetness and NH_3 levels. According to a summary of recent observations provided to EMEP (Smith et al. 2003), reasonable values for the canopy resistance of SO_2 in areas of low and high NH_3, and wet and dry conditions, can be summarised as:

Table 8.4: Basis of R_{ns} (s m^{-1}) scheme for SO_2

R_{ns}	Dry surfaces	Wet surfaces
High NH_3	80	40
Low NH_3	180	100

From (Smith et al. 2003)

In a first attempt to interpolate between these values, we make use of the acidity ratio a_{SN} defined by eqn. [8.15] and introduce a simple function F_{SN}:

$$\begin{aligned} F_{SN} &= e^{-(2-a_{SN})} & a_{SN} < 2 \\ &= 1 & a_{SN} \geq 2 \end{aligned} \tag{8.20}$$

This function returns values of 1.0, 0.61, 0.37 for a_{SN} ratios of 2.0, 1.5 and 1.0. If we define the basic dry and wet resistances, Rd = 180 s m^{-1}, Rw = 100 s m^{-1}, R_{ns} values for SO_2 are defined for both wet and dry surfaces:

$$\begin{aligned} R_{ns,dry}^{SO_2} &= Rd * F_{SN} + R_{low} + 2000\,\delta_{snow} \\ R_{ns,wet}^{SO_2} &= Rw * F_{SN} + R_{low} + 2000\,\delta_{snow} \end{aligned} \tag{8.21}$$

Giving $G_{ns,dry}^{SO_2}$ and $G_{ns,wet}^{SO_2}$ as the inverse values.

8.6.4 Extension to Other gases

For all gases other than HNO_3 or NH_3 we obtain G_{ns} by interpolating between the values for O_3 and SO_2. This interpolation borrows the solubility index, here denoted H_*, and the reactivity index, f_0, from the Wesely (1989) methodology, but these are applied directly now to total non-stomatal conductance rather than to individual resistances (Table 8.2). As there is so little data available on non-stomatal resistances, even for O_3 and SO_2, this simpler scaling seems acceptable. With these indices, the dry and wet conductance values for a gas i are obtained from the values for ozone and SO_2 using:

$$\begin{aligned} G_{ns,dry}^{i} &= 10^{-5} H_*^i\, G_{ns,dry}^{SO_2} + f_0^i\, G_{ns}^{O_3} \\ G_{ns,wet}^{i} &= 10^{-5} H_*^i\, G_{ns,wet}^{SO_2} + f_0^i\, G_{ns}^{O_3} \end{aligned} \tag{8.22}$$

8.6.5 Humidity effects

The so-called 'dry' values of G_{ns} are allowed to approach their 'wet' values when RH approaches 100%. We define a humidity factor:

$$\begin{aligned} F_{RH} &= (RH - RH_{lim})/(100 - RH_{lim}) && \text{if } RH > RH_{lim} \\ &= 1 && \text{if } RH \leq RH_{lim} \end{aligned} \quad (8.23)$$

Where RH_{lim} is set to 85% for forests and 75% for other canopies, loosely based upon results of wetness measurements presented in Klemm et al. (2002). The final equation applied to $G_{ns,dry}$ is then:

$$G_{ns,dry} = (1.0 - F_{RH})\, G_{ns,dry} + F_{RH}\, G_{ns,wet} \quad (8.24)$$

8.7 Canopy conductance - non-vegetative surfaces

For surfaces without vegetation canopies, the R_{gs} values are taken directly from the base $\hat{R}_{gs}$-values of Table 8.3 and adding the low-temperature and snow modifications:

$$\begin{aligned} R_{gs}^{O_3} &= \hat{R}_{gs}^{O_3} + R_{low} + 2000\, \delta_{snow} \\ R_{gs}^{SO_2} &= \hat{R}_{gs}^{SO_2} + R_{low} + 2000\, \delta_{snow} \end{aligned} \quad (8.25)$$

$$\begin{aligned} G_{ns,dry} &= 10^{-5} H^* / R_{gs,dry}^{SO_2} + f_0\, G_{ns}^{O_3} \\ G_{ns,wet} &= 10^{-5} H^* / R_{gs,wet}^{SO_2} + f_0\, G_{ns}^{O_3} \end{aligned} \quad (8.26)$$

8.8 Aerosol dry deposition

Aerosol dry deposition velocity at height z_{ref} is calculated as:

$$V_g = \frac{1}{R_a + R_b + R_a R_b v_s} + v_s \quad (8.27)$$

where v_s is the gravitational settling velocity. Other terms are as for gases. An assumption is made that all particles stick to the surface, so that the surface resistance R_c is set to zero.

The dry deposition velocity of atmospheric aerosols depends on their sizes. The Unified model distinguishes fine and coarse particles, which are presently assigned the diameters of 0.3 and 4 μ m. To account for a strong dependence of the mass average deposition velocity on the aerosol size distribution all the resistances are integrated over the aerosol sizes, assuming a log-normal particle size distribution with the geometric standard deviations of 2.0 and 2.2 μ m for fine and coarse particles respectively.

8.8.1 Gravitational settling, v_s

The gravitational settling velocity is calculated as

$$v_s = \frac{D_p^2 \rho_p g\, C_c}{18\ \mu} \tag{8.28}$$

here D_p and ρ_p are respectively the particle diameter and density, μ is the air dynamic viscosity, g is the gravitational acceleration, and C_c is the slip correction factor (Cunninghan correction factor) found as

$$C_c = 1 + \frac{2\lambda}{d_p}\left[1.257 + 0.4\exp\left(-\frac{1.1 d_p}{2\lambda}\right)\right] \tag{8.29}$$

here λ is the mean free path of gas molecules in air (λ = 0.065×10^{-6} m).

$$\mu = \nu \rho_{air} \tag{8.30}$$

where ν is the air kinematic viscosity ($\nu = 1.46 \times 10^{-5}$ m^2 s^{-1}) and ρ_{air} is the air density.

8.8.2 Quasi-laminar layer resistance, R_b

Depending on particle sizes, the viscous (quasi-laminar) layer resistance is largely controlled by processes of Brownian diffusion, interception and impaction. The formulation used depends on the underlying surface:

Smooth land surfaces (ice, desert) Following, e.g. Slinn et al. (1978), Seinfeld and Pandis (1998), we use:

$$R_b = \frac{1}{u_*(Sc^{2/3} + 10^{-3/St})} \tag{8.31}$$

where $u_*$is the friction velocity, *Sc* = ν/D is the Schmidt number, *St* is the Stokes number, $St = \frac{u_*^2 v_g}{g\,\nu}$, ν is the kinematic viscosity of air, and D is the Brownian diffusivity coeffi cient defi ned as

$$D = \frac{k\,T\,C_c}{3\pi\,\nu\,\rho_{air}\,D_p} \tag{8.32}$$

where k is the Boltzmann constant, T is the ambient temperature, ρ_{air} is the air density, and C_c is the slip correction factor, defi ned as above.

Deposition on vegetative surfaces

Based on Slinn (1980), the expression for quasi-laminar resistance over vegetation is written as

$$R_b = \frac{1}{u_*(1+0.24\frac{w_*^2}{u_*^2})\,(Sc^{-2/3}+\frac{\overline{St}}{1+\overline{St}^2})} \tag{8.33}$$

Here, w_* is the convective velocity scale for the PBL (Wesely et al. 1985) and calculated as $w_* = [g\,H\,z_i/(\rho\;C_p\theta)]^{2/3}$, where H is the sensitive heat flux, z_i is the mixed layer height. The average Stokes number is calculated as $St = \tau u_*/(c\hat{A}) = v_g u_*/(g\;c\;\hat{A})$, where c is a numerical factor, expected to be near unity, $\hat{A}$ is a characteristic "radius" of large collectors, e.g. grass blades, stalks, needles, etc. ($\hat{A}$ = 1mm). This parameterisation is applied for all vegetative snow free surfaces and for coniferous forests in all seasons.

For non-coniferous vegetation outside the growing period:

$$R_b = \frac{1}{u_*(1+0.24\frac{w_*^2}{u_*^2})\;\left(Sc^{-2/3}+10^{-3/St}\right)} \tag{8.34}$$

Deposition on water Two parameterisations for the resistance of quasi-laminar layer over seas are implemented.

1. The first one, based on the work by Slinn and Slinn (1980), accounts for the effect of wind and the fact that the surface of natural waters slips as compared to solid surfaces. Then,

$$R_b = \frac{\kappa \cdot u_h}{u_*^2}\frac{1}{(Sc^{-1/2}+10^{-3/St})} \tag{8.35}$$

where u_h is the wind speed at the reference height z_{ref} . Effects of bubble burst and aerosols capture by sea spray are not allowed for in this parameterisation.

2. The second parameterisation takes into account that over oceans, surfaces of quasi-laminar boundary layer can be disrupted by bursting bubbles. In those cases, the resistance is determined by turbulence and the washout velocity of particles by spray drops (van den Berg and Levieveld 2000):

$$R_b = \frac{1}{(1-\alpha_{bb})(v_B+v_i)+\alpha_{bb}(v_a+v_w)} \tag{8.36}$$

where α_{bb} is the relative area with bursting bubbles, v_B is the Brownian diffusion velocity, v_i is the impaction velocity, v_w is the washout velocity , and $v_a = 1/R_a$.

$$v_B = \frac{Cu_*}{\sqrt{Sc\cdot Re}} \tag{8.37}$$

where u_* is the friction velocity, *Sc* is the Schmidt number (see above), Re is the Reynolds number (*Re* = $u_* z_0/\nu$), ν is the air kinematic viscosity, and C is a constant (=1/3).

$$v_i = u_* 10^{-3/St} \tag{8.38}$$

where *St* is the Stokes number.

$$v_w = E_c(2\pi r_{sd}^2)(2z_d)F_{sd} \tag{8.39}$$

where E_c is the collection effi ciency (= 0.5) of the spray drops, $2\pi r_{sd}^2$ is the area of spray drops ($r_{sd} = 50\mu$ m), z_{sd} is the average height reached by the spray drops (= 50 m), and F_{sd} is the flux of spray drops ($= 5 \times 10^6 m^{-2} s^{-1}$). The area of bursting bubbles (α_{bb}) can be approximated by the area covered with whitecaps, which is

$$\alpha_{bb} = 1.7 \times 10^{-6} u_{10}^{3.75} \tag{8.40}$$

where u_{10} it the wind speed at 10 m height.

The latter parameterisation calculates greater deposition velocities of particles. Further tests on those two parameterisations for particle deposition velocities over seas are needed.

8.8.3 Bounce-off

Bounce-off of coarse particles from all dry surfaces is roughly accounted in the model based on the expression suggested by Slinn (1980). The reduction in collection effi - ciency of particle on the underlying surface, or rebound fraction, R, is calculated as

$$R = \exp(-b\sqrt{St}) \tag{8.41}$$

Here, St is the Stokes number (see above) and b is an experimental parameter (b=2). The underlying surface is assumed dry if no precipitation occurred during last three hours.

CHAPTER 9

Wet Deposition

Parameterisation of the wet deposition processes in the Unifi ed EMEP model includes both in-cloud and sub-cloud scavenging of gases and particles.

9.1 In-cloud scavenging

The in-cloud scavenging of a soluble component C is given by the expression:

$$\Delta C_{wet} = -C \frac{W_{in} \cdot P}{\Delta z \cdot \rho_w} \tag{9.1}$$

where W_{in} is the in-cloud scavenging ratio given in Table 9.1, P (kg m^{-2}s^{-1}) is the precipitation rate, Δz is the scavenging depth (assumed to be 1000 m) and ρ_w is the water density (1000 kg m^{-3}). We do not account for the effect that dissolved material may be released if clouds or rain water evaporate.

9.2 Below-cloud scavenging

For below cloud scavenging a distinction is made between scavenging of particulate matter and gas phase components. The sub-cloud scavenging of the gases is calculated as:

$$\Delta C_{wet} = -C \frac{W_{sub} \cdot P}{\Delta z \cdot \rho_w} \tag{9.2}$$

where W$_{sub}$ is the sub-cloud scavenging ratio given in Table 9.1.

Wet deposition rates for particles are calculated, based on Scott (1979), as:

Table 9.1: Wet scavenging ratios and collection efficiencies used in the Unified model.

Component	W_{in} (*10^6)	W_{sub} (*10^6)	E
SO_2	0.3	0.15	-
HNO_3	1.4	0.5	-
NH_3	1.4	0.5	-
H_2O_2	1.4	0.5	-
HCHO	0.1	0.03	-
SO_4^{2-}	1.0	-	0.1
NO_3^- fine	1.0	-	0.1
NH_4^+	1.0	-	0.1
$PPM_{2.5}$	1.0	-	0.1
NO_3^- coarse	1.0	-	0.4
PPM coarse	1.0	-	0.4

$$\Delta C_{wet} = -C\frac{A \cdot P}{V_{dr}} \cdot \bar{E} \tag{9.3}$$

where V_{dr} is the the raindrop fall speed (V_{dr}=5 m s^{-1}), A = 5.2 m^3 kg^{-1} s^{-1} is the empirical coefficient (a Marshall-Palmer size distribution is assumed for rain drops), and $\bar{E}$ is the size-dependent collection efficiency of aerosols by the raindrops (see Table 9.1).

References

J. Amundsen and R. Skålin. Gc user's guide release 1.3, 1995. Technical Report STF10 A95002, SINTEF Industrial Mathematics, Trondheim, Norway.

Y. Andersson-Sköld and D. Simpson. Comparison of the chemical schemes of the EMEP MSC-W and the IVL photochemical trajectory models, 1997. Norwegian Meteorological Institute, EMEP MSC-W Note 1/97.

Y. Andersson-Sköld and D. Simpson. Comparison of the chemical schemes of the EMEP MSC-W and the IVL photochemical trajectory models. *Atmospheric Environment*, 33:1111–1129, 1999.

Y. Andersson-Sköld and D. Simpson. Secondary organic aerosol formation in Northern Europe: a model study. *J. Geophys. Res.*, 106(D7):7357–7374, 2001.

R. Atkinson. Gas-phase troposheric chemistry of organic compounds: a review. *Atmospheric Environment*, 24A(1):1–41, 1990.

R. Atkinson, D.L. Baulch, R. A. Cox, R. F. Hampson, J.A. Kerr, M.J. Rossi, and J. Troe. Evaluated kinetic and photochemical data for atmospheric chemistry. Supplement V. IUPAC subcommittee on gas kinetic data evaluation for atmospheric chemistry. *Atmospheric Environment*, 57:on discette, 1996.

R. Atkinson, D.L. Baulch, R.A. Cox, R.F. Hampson, J.A. Kerr, and J. Troe. Evaluated kinetic and photochemical data for atmospheric chemistry: supplement IV. *Atmospheric Environment*, 26A(7):1187–1230, 1992.

A. Benedictow. Documentation and verifi cation of the 1999 PARLAM-PS meteorological fi elds used as input for Eulerian EMEP model. Technical report, Norwegian Meteorologial Institute, Oslo, Norway, 2003. Research Note no. 111. (Reports also available for 1980,1985,1995,1999, and 2000, see `www.emep.int`).

E. Berge and H. A. Jakobsen. A regional scale multi-layer model for the calculation of long-term transport and deposition of air pollution in Europe. *Tellus*, 50:205–223, 1998.

D. Bjørge and R. Skålin. PARLAM - the parallel HIRLAM version at DNMI, 1995. Research Report No. 27, ISSN 0332-9879 Norwegian Meteorological Institute, Oslo, Norway.

A. K. Blackadar, 1979. High resolution models of the planetary boundary layer. Advances in environment and scientifi c engineering. London: Gordon and Breach.

R.J. Bojkov. Surface ozone concentrations during the second half of the nineteenth century. *J. Clim. appl. Met.*, 25:343–352, 1986.

A. Bott. A positive defi nite advection scheme obtained by non-linear re-normalization of the advection fluxes. *Mon. Weather Rev.*, 117:1006–1015, 1989a.

A. Bott. Reply. *Mon. Weather Rev.*, 117:2633–2636, 1989b.

J. A. Businger, J. C. Wyngaard, Y. Izumi, and E. F. Bradley. Flux-profi le relationship in the atmospheric boundary layer. *J. of Atmospheric Sciences*, 28:181–189, 1971.

P.A.M. de Smet and J.-P. Hettelingh. Intercomparison of Current Landuse/Land Cover Databases. In M. Posch, P.A.M. de Smet, J.-P. Hettelingh, and R.J. Downing, editors, *Modelling and Mapping of Critical Thresholds in Europe. Status report 2001*. Coordination Centre for Effects, RIVM, Bilthoven, The Netherlands, 2001.

W.B. DeMore, D.M. Sander, S.P. amd Golden, R.F. Hampson, M.J. Kurylo, C.J. Howard, A.R. Ravishankara, C.E. Kolb, and M.J. Molina. Chemical kinetics and photochemical data for use in stratospheric modelling, 1997. JPL Publication 97-4.

F.J. Dentener and P.J. Crutzen. Reaction of N_2O_5 on tropospheric aerosols: Impact on the global distributions of NO_x O_3 and OH. *J. Geophys. Res.*, 98:7149–7163, 1993.

R.G. Derwent, P.G. Simmonds, S. Seuring, and C. Dimmer. Observations and interpretation of the seasonal cycles in the surface concentrations of ozone and carbon monoxide at Mace Head, Ireland from 1990 to 1994. *Atmospheric Environment*, 32: 145–157, 1998.

M. U. Dutsch. The ozone distribution in the atmosphere. *Can. J. Chem.*, 52:1491–1504, 1974.

J. Duyzer and D. Fowler. Modelling land atmosphere exchange of gaseous oxides of nitrogen in Europe. *Tellus*, 46B:353–372, 1994.

U. Ehhalt, D.H.and Schmidt, R. Zander, Ph. Demoulin, and C.P. Rinsland. Seasonal cycle and secular trend of the total and tropospheric column abundance of ethane above the Jungfraujoch. *J. Geophys. Res.*, 96:4985–4994, 1991. D3.

A. Eliassen, Ø. Hov, I.S.A. Isaksen, J. Saltbones, and F. Stordal. A lagrangian long-range transport model with atmospheric boundary layer chemistry. *J. Appl. Met.*, 21 (11):1645–1661, 1982.

L. Emberson, D. Simpson, J.-P. Tuovinen, M.R. Ashmore, and H.M. Cambridge. Towards a model of ozone deposition and stomatal uptake over Europe, 2000a. EMEP MSC-W Note 6/2000.

L. Emberson, G. Wieser, and M.R. Ashmore. Modelling of stomatal conductance and ozone flux of Norway spruce: comparison with fi eld data. *Environmental Pollution*, 109(3):393–402, 2000b.

L.D. Emberson, M.R. Ashmore, D. Simpson, J.-P. Tuovinen, and H.M. Cambridge. Modelling and mapping ozone deposition in Europe. *Water, Air and Soil Pollution*, 130:577–582, 2001.

L.K. Emmons, D. Hauglustaine, J.-F. Müller, M.A. Carroll, G.P. Brasseur, D. Brunner, J. Staehelin, V. Thouret, and A. Marenco. Data composites of airborne observations of tropospheric ozone and its precursors. *J. Geophys. Res.*, 105(D16):20497–20538, 2000.

J. W. Erisman, A. Hensen, D. Fowler, C. R. Flechard, A. Grüner, G. Spindler, J. H. Duyzer, H. Weststrate, F. Römer, A. W. Vonk, and H. V. Jaarsveld. Dry deposition monitoring in europe. *Water, Air and Soil Pollution, Focus*, 1:17–27, 2001.

J.W. Erisman, A. van Pul, and P. Wyers. Parameterization of surface resistance for the quantifi cation of atmospheric deposition of acidifying pollutants. *Atmospheric Environment*, 28:2592–2607, 1994.

H. Fagerli and A. Eliassen. Modifi ed parameterisation for vertical diffusion, 2002. In EMEP MSC-W Report 1&2/2002, Transboundary Acidifi cation, Eutrophication and Ground Level Ozone in Europe. EMEP Summary Report 2002. Norwegian Meteorological Institute, Oslo, Norway.

J. P. F Fortuin and H. Kelder. An ozone climatology based on ozonesonde and satellite measurements. *J. Geophys. Res.*, 103:31,709–31,734, 1998.

D. Fowler and J.W. Erisman. Biosphere/Atmosphere Exchange of Pollutants. Overview of subproject BIATEX-2. In Midgley, P.M. and Reuther, M., editor, *Towards Cleaner Air for Europe – Science, Tools and Applications, Part 2. Overviews from the Final Reprots of the EUROTRAC-2 Subprojects*. Margraf Verlag, Weikersheim, 2003. Also available frm `http://www.gsf.de/eurotrac/publications/`.

R.M. Gardner, K. Adams, T. Cook, F. Deidewig, S. Ernedal, R. Falk, E. Fleuti, E. Herms, C.E. Johnson, D.S. Lee M. Lecht, M. Leech, D. Lister, B. Masse, M. Metcalfe, P. Newton, A. Schmitt, C. Vandenbergh, and R. Van Drimmelen. The ANCAT/EC global inventory of NO_x emissions from aircraft. *Atmospheric Environment*, 31(12):1751–1766, 1997.

J.R. Garratt. *The atmospheric boundary layer*. Cambridge University Press, Cambridge, England, 1992.

A. Guenther, P. Zimmerman, and M. Wildermuth. Natural volatile organic compound emission rate estimates for U.S. woodland landscapes. *Atmospheric Environment*, 28:1197–1210, 1994.

A.B. Guenther, P.R. Zimmerman, P.C. Harley, R.K. Monson, and R. Fall. Isoprene and monoterpene rate variability: model evaluations and sensitivity analyses. *J. Geophys. Res.*, 98(D7):12609–12617, 1993.

Ø. Hov, A. Eliassen, and D. Simpson. Calculation of the distribution of NO_x compounds in Europe. In I.S.A. Isaksen, editor, *Troposheric ozone. Regional and global scale interactions*, pages 239–262, Dordrecht, 1988. D. Reidel.

I.S.A. Isaksen and Ø Hov. Calculation of trends in the tropospheric concentration of O_3, OH, CO, CH_4 and NO_x. *Tellus*, 39B:271–285, 1987.

T. Iversen. Calculations of long-range transported sulphur and nitrogen over Europe. *Science of the Total Environment*, 96:87–99, 1990.

T. Iversen and T. E. Nordeng. A numerical model suitable for the simulation of a broad class of circulation systems on the atmospheric mesoscale. Technical Report 2, Norwegian Institute for Air Research, Kjeller, Norway, 1987.

H. A. Jakobsen, E. Berge, T. Iversen, and R. Skålin. Status of the development of the multi-layer Eulerian model: a) Model description, b) A new method of calculating mixing heights, c) Model results for sulphur transport and deposition in Europe for 1992 in the 50 km grid. EMEP/MSC-W Note 3/95, The Norwegian Meteorological Institute, Oslo, Norway, 1995.

W.E. Janach. Surface ozone: trend details, seasonal variations, and interpretation. *J. Geophys. Res.*, 94:18289–18295, 1989. D15.

J. E. Jonson, L Tarrasón, J.K. Sundet, T. Berntsen, and S. Unger. The Eulerian 3-D oxidant model: Status and evaluation for summer 1996 results and case-studies. In *Transboundary photo-oxidant air pollution in Europe.* EMEP/MSC-W Status Report 2/98, The Norwegian Meteorological Institute, Oslo, Norway, 1998.

J.E. Jonson, H.A. Jakobsen, and E. Berge. Status of the development of the regional scale photo-chemical multi-layer Eulerian model, 1997. Norwegian Meteorological Institute, EMEP MSC-W Note 2/97.

J.E. Jonson, A. Kylling, T. Berntsen, I.S.A. Isaksen, C.S. Zerefos, and K. Kourtidis. Chemical effects of UV fluctuations inferred from total ozone and tropospheric aerosol variations. *J. Geophys. Res.*, 105:14561–14574, 2000.

J.E. Jonson, J.K. Sundet, and L.Tarrasón. Model calculations of present and future levels of ozone and ozone precursors with a global and a regional model. *Atmospheric Environment*, 35:525–537, 2001.

O. Klemm, C. Milford, M.A. Sutton, G. Spindler, and E. Van Putton. A climatology of leaf surface wetness. *Theor. Appl. Climatol.*, 71:107–117, 2002.

I. Köhler, R. Sausen, and G. Klenner. NO_x production from lightning. The impact of NO_x emissions from aircraft upon the atmosphere at flight altitudes 8-15 km (AERONOX), edited by U.Schumann, fi nal report to the Commission of the European Communities, Deutch Luft und Raumfart, Oberpfaffenhofen, Germany, 1995.

M. Kuhn, P.J.H. Builtjes, D. Poppe, D. Simpson, W.R. Stockwell, Y. Andersson-Sköld, A. Baart, M. Das, F. Fiedler, Ø. Hov, F. Kirchner, P.A. Makar, J.B. Milford, M.G.M. Roemer, R. Ruhnke, A. Strand, B. Vogel, and H. Vogel. Intercomparison of the gas-phase chemistry in several chemistry and transport models. *Atmospheric Environment*, 32(4):693–709, 1998.

A. Kylling, A. F. Bais, M. Blumthaler, J. Schreder, C. S. Zerefos, and E. Kosmidis. The effect of aerosols on solar UV irradiances during the Photochemical Activity and Solar Radiation campaign. *J. Geophys. Res.*, 103:21051–26060, 1998.

J. A. Logan. An analysis of ozonesonde data for the troposhere: Recommendations for testing 3-d models and development of a gridded climatology for troposheric ozone. *J. Geophys. Res.*, 10(D13):16,115–16,149, 1998.

J.A. Logan. Trends in the vertical distribution of ozone: An analysis of ozonesonde data. *J. Geophys. Res.*, 99(D12):25553–25585, 1994.

P.S. Low, T.D. Davies, P.M. Kelly, and G. Farmer. Trends in surface ozone at Hohenpeissenberg and Arkona. *J. Geophys. Res.*, 95:22441–22453, 1990. D13.

L. R. Martin and D. E. Damschen. Aqueous oxidation of sulphur dioxide by hydrogen peroxide at low p. *Atmospheric Environment*, 15:1615–1621, 1981.

D. Möller. Kinetic model of atmospheric SO_2 oxidation based on published dat. *Atmospheric Environment*, 14:1067–1076, 1980.

M. Mozurkewich. The dissociation constant of ammonium nitrate and its dependence on temperature, relative humidity and particle size. *Atmospheric Environment*, 27a: 261–270, 1993.

E. Nemitz, C. Milford, and M. A. Sutton. A two-level canopy compensation point model for describing bi-directional biosphere-atmosphere exchange of ammonia. *Q. J. R. Meteorol. Soc.*, 127:815–833, 2001.

T.E. Nordeng. Parameterization of physical processes in a three-dimensional numerical weather prediction model, 1986. Norwegian Meteorological Institute Technical Report No. 65, Oslo, NOrway.

J. J. O'Brien. A note on the vertical structure of the eddy exchange coeffi cient in the planetary boundary layer. *J. of Atmospheric Sciences*, 27:1213–1215, 1970.

K. Olendrzyński, J.E. Jonson, J. Bartnicki, H.A. Jakobsen, and E. Berge. EMEP Eulerian model for acid deposition over Europe. *Int. J. of Environmental Technology and Management*, in press, 2000.

S.A. Penkett, N.J. Blake, P. Lightman, A.R.W. Marsh, P. Anwyl, and G. Butcher. The seasonal variation of nonmethane hydrocarbons in the free troposphere over the North Atlantic ocean: possible evidence for extensive reaction of hydrocarbons with the nitrate radical. *J. Geophys. Res.*, 98(D2):2865–2885, 1993.

R.A.Sr. Pielke. *Mesoscale meteorological modelling. Second Edition*. Academic Press, 2002.

PORG. *Ozone in the United Kingdom 1993*. UK Dept. of the Environment, London, UK, 1993. Third Report of the United Kingdom Photochemical Oxidants Review Group.

M. Posch, P.A.M. de Smet, J.-P. Hettelingh, and R.J. Downing, editors. *Modelling and Mapping of Critical Thresholds in Europe. Status report 2001*. Coordination Centre for Effects, RIVM, Bilthoven, The Netherlands, 2001.

S. Reis, D. Simpson, R. Friedrich, J.E. Jonson, S. Unger, and A. Obermeier. Road traffi c emissions - predictions of future contributions to regional ozone levels in Europe. *Atmospheric Environment*, 34:4701–4710, 2000.

H. Sandnes Lenschow and S. Tsyro. Meteorological input data for EMEP/MSC-W air pollution models, 2000. EMEP MSC-W Note 2/2000.

B. C. Scott. Parameterization of sulphate removal by precipitation. *J. Appl. Met.*, 17: 11375–11389, 1979.

J.H. Seinfeld and S.N. Pandis. *Atmospheric chemistry and physics. From air pollution to climate change* . John Wiley and Sons, inc., New York, 1998.

R. Shapiro. Smoothing, filtering and boundary effects. *Rev. Geophys. Space Phys.*, 8: 359–387, 1970.

D. Simpson. Long period modelling of photochemical oxidants in Europe. Calculations for July 1985. *Atmospheric Environment*, 26A(9):1609–1634, 1992.

D. Simpson. Photochemical model calculations over Europe for two extended summer periods: 1985 and 1989. Model results and comparisons with observations. *Atmospheric Environment*, 27A(6):921–943, 1993.

D. Simpson. Biogenic emissions in Europe 2: Implications for ozone control strategies. *J. Geophys. Res.*, 100(D11):22891–22906, 1995.

D. Simpson, Y. Andersson-Sköld, and M. E. Jenkin. Updating the chemical scheme for the EMEP MSC-W oxidant model : current status, 1993. Norwegian Meteorological Institute, EMEP MSC-W Note 2/93.

D. Simpson, H. Fagerli, S. Solberg, and W. Aas. Photo-oxidants, 2003a. In, EMEP MSC-W Report 1/2003, Part II, Unified EMEP Model performance. Norwegian Meteorological Institute, Oslo, Norway.

D. Simpson, A. Guenther, C.N. Hewitt, and R. Steinbrecher. Biogenic emissions in Europe 1. Estimates and uncertainties. *J. Geophys. Res.*, 100(D11):22875–22890, 1995.

D. Simpson, J.-P. Tuovinen, L.D. Emberson, and M.R. Ashmore. Characteristics of an ozone deposition module. *Water, Air and Soil Pollution, Focus*, 1:253–262, 2001.

D. Simpson, J.-P. Tuovinen, L.D. Emberson, and M.R. Ashmore. Characteristics of an ozone deposition module ii: sensitivity analysis. *Water, Air and Soil Pollution*, 143: 123–137, 2003b.

D. Simpson, W. Winiwarter, G. Börjesson, S. Cinderby, A. Ferreiro, A. Guenther, C. N. Hewitt, R. Janson, M. A. K. Khalil, S. Owen, T. E. Pierce, H. Puxbaum, M. Shearer, U. Skiba, R. Steinbrecher, L. Tarrasón, and M. G. Öquist. Inventorying emissions from nature in Europe. *J. Geophys. Res.*, 104(D7):8113–8152, 1999.

R. Skålin, I. Lie, and E. Berge. A parallel algorithm for simulation of long range transport of air pollution. In F.-X. Le Dimet, editor, *High performance computing in the geosciences*, pages 175–185. Kluwer Academic Publishers, 1995.

S. A. Slinn and W. G. N. Slinn. Prediction for particle deposition on natural waters. *Atmospheric Environment*, 14:1013–1016, 1980.

W. G. N. Slinn. Prediction for particle deposition to vegetable surfaces. *Atmospheric Environment*, 16:1785–1794, 1980.

W. G. N. Slinn, L. Hasse, B. B. Hicks, A. W. Hogan, D. Lal, P. S. Liss, K. O. Munnich, G. A. Sehmel, and O. Vittori. Review paper: Some aspects of the transfer of atmospheric trace constituents past the air-sea interface. *Atmospheric Environment*, 12: 2055–2087, 1978.

R. Smith, D. Fowler, and M. A. Sutton. The external surface resistance in the EMEP Eulerian model, 2003. Unpublished Note, Centre for Ecology and Hydrology, Penicuik, Scotland.

R. Smith, D. Fowler, M. A. Sutton, C. Flechard, and M. Coyle. Regional estimation of pollutant gas dry deposition in the UK: model description, sensitivity analyses and outputs. *Atmospheric Environment*, 34:3757–3777, 2000.

S. Solberg, C. Dye, N. Schmidbauer, A. Herzog, and R. Gehrig. Carbonyls and nonmethane hydrocarbons at rural European sites from the Mediterranean to the Arctic. *J. Atmos. Chem.*, 25:33–66, 1996.

S. Solberg, C. Dye, S.E. Walker, and D. Simpson. Long-term measurements and model calculations of formaldehyde at rural European monitoring sites. *Atmospheric Environment*, 35(2):195–207, 2000.

Frode Stordal, Ivar S. A Isaksen, and Kjell Horntveth. A diabatic circulation two–dimensional model with photochemistry: simulations of ozone and long–lived tracers with surface sources. *J. Geophys. Res.*, 90:5757–5776, 1985.

R.B. Stull. *An introduction to Atmospheric Boundary Layer Meteorology*. Kluwer Academic Publishers, Dordrecht, 1988.

J.K. Sundet. *Model studies with a 3-d global CTM using ECMWF data*. PhD thesis, Department of Geophysics, University of Oslo, Norway, 1997.

L. Tarrasón, S. Turner, and I. Floisand. Estimation of seasonal dimethyl sulphide fluxes over the North Atlantic Ocean and their contribution to European pollution levels. *J. Geophys. Res.*, 100:11623–11639, 1995.

Tarrasón, L. (ed). EMEP Report 1/2003, Transboundary Acidification, Eutrophication and Ground Level Ozone in Europe. Part II, Unified EMEP Model Performance, 2003. EMEP Status Report 2003, Norwegian Meteorological Institute, Oslo, Norway.

J.-P. Tuovinen, M.R. Ashmore, L.D. Emberson, and D. Simpson. Testing and improving the EMEP deposition module, 2003. Submitted.

J.-P. Tuovinen, D. Simpson, T.N. Mikkelsen, L.D. Emberson, M. R. Ashmore M., Aurela, H. M. Cambridge, M. F. Hovmand, N. O. Jensen, T. Laurila, K. Pilegaard, and H. Ro-Poulsen. Comparisons of measured and modelled ozone deposition to forests in Northern Europe. *Water, Air and Soil Pollution, Focus*, 1:263–274, 2001.

UNECE. International Cooperative Programme on Modelling and Mapping of Critical Loads & Levels and Air Pollution Effects, Risks and Trends. Manual on Methodologies and Criteria for Mapping Critical Levels/Loads and geographical Areas where they are exceeded, 2003. To be published. See `www.oekodata.com/icpmapping/html/manual.htm`.

F. van den Berg, A.and Dentener and J. Levieveld. Modelling of chemistry of the marine boundary layer: Sulphate formation and the role of sea salt aerosol particles. *J. Geophys. Res.*, 105(D9):11,671–11,698, 2000.

J.G. Verwer and D. Simpson. Explicit methods for stiff ODEs from atmospheric chemistry. *Applied Numerical Mathematics*, 18:413–430, 1995.

V. Vestreng. Review and Revision. Emission data reported to CLRTAP. EMEP MSC-W Status Report 2003. Technical Report Note 1/2003, Meteorological Synthesizing Centre - West, Norwegian Meteorological Institute, Oslo, Norway, 2003.

A. Volz and D. Kley. Evaluation of the Montsouris series of ozone measurements made in the nineteenth century. *Nature*, 332:240–242, 1988.

S. Walton, M.W. Gallagher, T.W. Choularton, and J. Duyzer. Ozone and NO_2 exchange to fruit orchards. *Atmospheric Environment*, 31(17):2767–2776, 1997.

P. Warneck. *Chemistry of the Natural Atmosphere*. Academic Press, Inc., San Diego, California, 1988.

M. L. Wesely, D. R. Cook, R. L. Hart, and R. E Speer. Measurements and Parameterization of Particulate Sulfur Dry Deposition over Grass. *J. Geophys. Res.*, 90(D1): 2131–2143, 1985.

M.L. Wesely. Parameterization of surface resistances to gaseous dry deposition in regional scale numerical models. *Atmospheric Environment*, 23:1293–1304, 1989.

P. Wind, L. Tarrasón, E. Berge, L.H. Slørdal, S. Solberg, and S.-E. Walker. Development of a modeling system able to link hemispheric- regional and local air pollution problems, 2002. MSC-W Note 5/2002, Draft.

R. Zander, Ph. Demoulin, and U. Ehhalt, D.H.and Schmidt. Secular increase of the total vertical column abundance of methane derived from IR solar spectra recorded at the Jungfraujoch station. *J. Geophys. Res.*, 94:11029–11039, 1989a. D8.

R. Zander, Ph. Demoulin, U. Ehhalt, D.H.and Schmidt, and C.P. Rinsland. Secular increase of the total vertical column abundance of carbon dioxide above central Europe since 1950. *J. Geophys. Res.*, 94:11021–11028, 1989b. D8.

APPENDIX A

Aerosol Dynamics Model (UNI-AERO)

A.1 Introduction

The EMEP aerosol model (UNI-AERO) describes emissions, chemical transformation, dynamics, transport, and dry and wet deposition of atmospheric aerosol. The aerosol model considers primary and secondary aerosols. Primary particles are those directly emitted in the atmosphere, while secondary aerosols are formed in the atmosphere through gas-to-particle conversion.

The aerosol model includes 14 chemical prognostic components:

- Gases – SO_2, H_2SO_4, NO, NO_2, HNO_3, PAN, NH_3;
- Aerosols – SO_4, NO_3, NH_4, organic carbon(OC), elemental carbon (EC), mineral dust, sea salt (NaCl);
- Aerosol liquid water is a diagnostic component.

Secondary Organic Aerosols (SOA) and re-suspended and wind eroded mineral dust are not presently accounted for in the model.

UNI-AERO describes the aerosol size distribution with four modes: nucleation (particles with diameters d<0.02μm), Aitken (0.02μm<d<0.1μm), accumulation (0.1μm<d<2.5μm), and coarse (d<10.0μm). All particles within each mode are assumed to have the same size (monodisperse) and chemical composition (internally mixed aerosols) (Table A1). A flexible design of the aerosol model allows to easily modify the definitions of size modes.

UNI-AERO calculates particle mass and number distributed in the four modes, aerosol chemical composition, as well as the concentrations of $PM_{2.5}$ and PM_{10}. UNI-AERO can also calculate other PM concentrations, e.g. PM_1 if required. The present

Table A:1: Prognostic variables in MM32: N-number and M-mass concentration. (element present (X) or may be present (O) in the mode)

	N	M SO4	M NO3	M NH4	M EC	M OC*	M Dust**	M Sea salt	Water
Nucleation D<0.02 μm	X	X				O			
Aitken 0.02<D<0.1 μm	X	X	X	X	X	X	O	X	Diagnostic parameter
accumulation 0.1<D<2.5 μm	X	X	X	X	X	X	X	X	
coarse 2.5 <D< 10 μm	X	X	X	O			X	X	

*) Only primary OC is currently considered

**) Only anthropogenic mineral dust is currently considered

version of UNI-AERO solves 29 prognostic equations (7 for gases, 4 for particle numbers and 18 for particle masses). The EMEP aerosol model is quite cost-effi cient in terms of CPU usage.

A.2 Emissions

A.2.1 Primary anthropogenic $PM_{2.5}$ and PM_{10} emissions

Primary $PM_{2.5}$ and PM_{10} emissions are disaggregated into 10 source sectors and over the EMEP grid and distributed vertically as described in section 4.1. Chemical speciation of $PM_{2.5}$ emissions into organic carbon (OC), elemental carbon (EC) and inorganic components is based upon the source presented in Andersson-Sköld and Simpson (2001). OC and EC emissions are further distributed between Aitken and accumulation modes. Different tests were made where from 15 to 20% of $PM_{2.5}$ mass is assigned to the Aitken and from 85 to 80% to the accumulation mode (e.g. Seinfeld and Pandis 1998, Berdowski et al. 1997). Since no appropriate chemical speciation of PM emissions is presently available, the inorganic components in UNI-AERO are presently assumed to be mineral dust. All mineral dust from $PM_{2.5}$ emissions is assigned to the accumulation mode (Table A:2).

Emissions of coarse particles are calculated as the difference between PM_{10} and $PM_{2.5}$ emissions. Primary coarse PM is assumed to consist of dust particles and assigned to the coarse mode. Table A:2 summarises the assumptions on the chemical composition and size distribution of $PM_{2.5}$ and PM_{10} emission presently adopted in UNI-AERO.

Particles number emissions in the Aitken, accumulation and coarse modes are de-

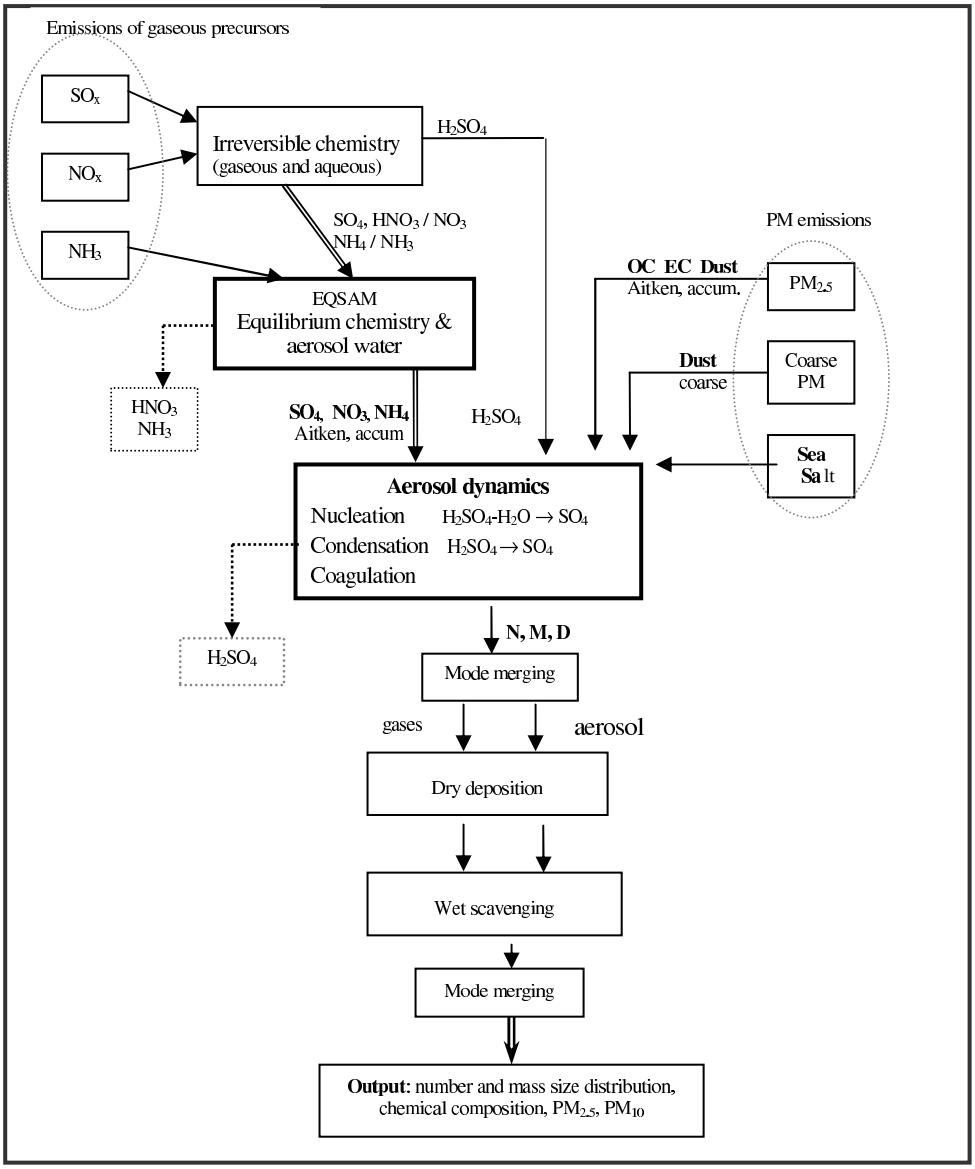

Figure A.1: Schematic computational structure of the EMEP aerosol model (advection and diffusion is not shown here).

rived from the mass emissions in the corresponding modes as

$$EmN_i = \frac{6}{\pi} \cdot \frac{EmM_i}{\rho_i D_i^3} \tag{A.1}$$

where EmN_i is the particle number emission in the mode i (m^{-3} s^{-1}), EmM_i is the particle mass emission in the mode i(kg m^{-3} s^{-1}), D_i is the average diameter of particles emitted in the mode i (m), and ρ_i is the average particle density (kg m^{-3}), found as the mass weighted mean density of aerosol components present in the mode.

Table A:2: Size and chemical speciation of primary PM emission (in %) and component densities (kg/m^3) used in UNI-AERO

$PM_{2.5}$ Source sectors	**OC**	**EC**	**Inorganics (Mineral dust)**
Power generation	33	33	33
Non-industrial combustion	50	20	30
Industrial combustion	33	33	33
Production processes	0	20	80
Extraction & distribution of fossil fuels	40	50	10
Solvent and other product use	40	20	40
Road transport	40	20	40
Other mobile sources and machinery	40	20	40
Waste treatment and disposal	10	60	30
Agriculture	70	0	30
Size distribution (Aitken/accum) (%)	15/85 (20/80)	15/85 (20/80)	0 / 100
Coarse PM (PM_{10}- $PM_{2.5}$)	-	-	100
Density, ρ (kg/m^3)	2000	2200	2600

Diameters of primary emitted particles tested are 0.03-0.05μm for Aitken mode, 0.2-0.5 μm for accumulation mode and 4-5 μm for coarse mode. The same assumptions on emissions size distribution and particle sizes are applied for all emission sources and countries.

A.2.2 Sea salt generation

The generation of sea salt aerosol over oceans is driven by the surface wind. There are two main mechanisms for sea salt aerosol generation: bubble bursting during white-cap formation (indirect) and through spume drops under the wave breaking (direct). The latter mechanism is believed to be important source for particles larger than 10 μm and at wind speeds exceeding 10-12 m/s and therefore not considered here. Two parameterisation schemes for sea salt spray generation are implemented in the aerosol model.

1. The first parameterisation of the generation of sea salt aerosols through bubble bursting uses the empirical expression from Monahan et al. (1986):

$$\frac{dF}{dr_w} = 1.373 \cdot U_{10}^{3.41}\, r_w^{-3} \left(1 + 0.057 r_w^{1.05}\right) \cdot 10^{1.19\exp(-B^2)} \qquad \text{(A.2)}$$

where dF/dr_w is the rate of sea salt droplet generation per unit area of sea surface and per increment of droplet "wet" radius, r_w is the aerosol wet radius at 80 % relative

humidity, U_{10} is the wind speed at 10m, and *B=(0.380-log(r_w)/0.650.* This parameterisation is employed to calculate the generation of sea salt aerosol larger than r_w= 0.8 μm (or particles with dry diameters exceeding ca. 1-2 μm).

2. The second parameterisation for the generation of sea salt aerosols with dry diameters smaller than 1-2 μm is from work by Mårtensson et al. (2003).

$$\frac{dF}{d\log D_d} = 3.84 \cdot 10^{-6} \left(A_k T_w + B_k\right) \cdot U_{10}^{3.41} \tag{A.3}$$

where *dF/d(*logD_d) is the flux of sea salt particle per unit area of the whitecap cover and per increment of (log D_d), D_d is the dry diameter, T_w is the temperature of sea water (constant T_w=280 K was used for now), and A_k and B_k describes the size dependence of F:

$$\begin{aligned} A_k &= c_4 D_d^4 + c_3 D_d^3 + c_2 D_d^2 + c_1 D_d + c_0 \\ B_k &= d_4 D_d^4 + d_3 D_d^3 + d_2 D_d^2 + d_1 D_d + d_0 \end{aligned} \tag{A.4}$$

and the empirical coeffi cient c_i and d_i are tabulated.

A.3 Chemistry

The aerosol model is based on the simplifi ed SO_x-NO_x chemistry of the Acid Deposition model (Chapter 7 in this report).

A.3.1 Sulphate production

Differently from UNI-OZONE and UNI-ACID, UNI-AERO treats separately gaseous sulphuric acid (H_2SO_4), formed through gas-phase reactions, and sulphate aerosol (SO_4) due to aqueous phase formation.

Gaseous H_2SO_4 is formed in the model in the gas-phase oxidation of SO_2 by hydroxyl radical OH. $H_2SO_{4(g)}$ contributes to the formation of new particles through homogenous nucleation and to the increase of SO_4 aerosol mass due to condensation on pre-existing particles. The continuity equation for gaseous $H_2SO_{4(g)}$ can schematically be written as:

$$\frac{d(H_2SO_{4(g)})}{dt} = EmSO_4 + chem(H_2SO_4) - nucl - cond - Ddep_{H2SO4} - Wdep_{H2SO4}$$

Here *EmSO*$_4$ designates the fraction of SO_x emissions in the form of H_2SO_4 (presently 5 %), *chem(*H_2SO_4) is the rate of H_2SO_4 production due to oxidation of SO_2 by OH, *nucl* and *cond* are the loss rates of H_2SO_4 due to nucleation and condensation onto pre-existing particles and *Ddep*$_{H2SO4}$ and *Wdep*$_{H2SO4}$ are the rates of H_2SO_4 dry and wet deposition.

In clouds, the aqueous phase oxidation of SO_2 by H_2O_2 and O_3, which takes place in cloud droplets formed on atmospheric particles, forms particulate sulphate. Most SO_4 mass produced is accociated with the accumulation mode particles, which get activated effi ciently. A much smaller fraction of Aitken particles compared to accumulation particles gets activated, but they gain water becoming interstitial aerosols. Even though the lifetime of interstitial aerosols can be rather short as they get scavenged by the cloud droplets, they contain a signifi cant amount of water thus facilitating aqueous phase reactions. In clouds, this is believed to be the main mechanism of Aitken particles growth to the accumulation mode (see section A.6).

A.3.2 Gas/aerosol partitioning

The new version of the Equilibrium Simplifi ed Aerosol Model, EQSAM (Metzger et al. (2002) and pers. comm.), has recently been implemented in the aerosol model. EQSAM allows in a computationally effi cient way to calculate partitioning of volatile components between gas and aerosol phases. Compared to the previous EQSAM version implemented also in the Unifi ed model, more accurate parameterisations to calculate the aerosol molalities and the solute activity coeffi cients are included in the latest EQSAM (according to the appendix of (Metzger et al. 2002).

The main assumption made in EQSAM is that volatile species in the gas and aerosol phases are in chemical and thermodynamical equilibruim. Then, the aerosol activity (or aerosol molality) and hence the chemical composition is governed by the relative humidity. Based on the cation/anion mole ratios ([Na]+[NH_3]+[NH_4])/[SO_4], the entire set of possible aerosol compositions is devided in concentration domains. Each domain represents a certain aerosol type and is further subdivided into several sub-domains, according the the regime of deliquescence relative humidity for the corresponding aerosol composition. Assumption on metastable aqueous aerosols is adopted.The aerosol water content is calculated basen on the semi-empirical so-called ZSR-relation. The chemical composition of aerosol (i.e. aerosol/gas partitioning) is found from aerosol chemical equilibrium, which is determined by the temperature dependent equilibrium coeffi cient K(T).

In addition to nitrate and ammonium, the new EQSAM version was extended to include Na^+ and Cl^- from sea salt spray, so that a thermodynamic equilibrium of SO_4^{2-}-NO_3^--NH_4^+-Na^+-Cl^--H_2O system is considered. In this way, EQSAM accounts for the formation of coarse NO_3^- on the sea salt aerosols ($NaNO_3$) in addition to fi ne NO_3^- associated with ammonium nitrate (NH_4NO_3).

A.4 Aerosol dynamics

The aerosol dynamics module MM32 (Pirjola et al. 2003, Pirjola and Kulmala 2000) accounts in the aerosol model for particle nucleation, condensation and coagulation processes.

The differential equations for the evolution of particle **number** in all modes due to aerosol dynamic processes are:

$$\begin{aligned}
\delta N_1/\delta t &= Inuc - 0.5K_{11}N_1^2 - K_{12}N_1N_2 - K_{13}N_1N_3 - K_{14}N_1N_4 \\
\delta N_2/\delta t &= -0.5K_{22}N_2^2 - K_{23}N_2N_3 - K_{24}N_2N_4 \\
\delta N_3/\delta t &= -0.5K_{33}N_3^2 - K_{34}N_3N_4 \\
\delta N_4/\delta t &= -0.5K_{44}N_4^2
\end{aligned} \tag{A.5}$$

Here N_i (cm^{-3}) is the particles number concentration in the mode i, $Inuc$ (cm^{-3} s^{-1}) is the nucleation rate, K_{ij} (cm^3 s^{-1}) is the coagulation coeffi cient between particles in i and j modes ($i = j$ means coagulation of particles in the same mode, i.e. intramode coagulation, and $i \neq j$ means coagulation of particles from different modes, i.e. intermode coagulation). Indexes i=1, 2, 3, 4 refer to the nucleation, Aitken, accumulation and coarse mode, respectively.

Equations for the evolution of **mass concentration** due to aerosol dynamics are written for all aerosol components present in each of four size modes. As an example, evolution equations for SO_4 mass are given here:

$$\begin{aligned}
\delta M_1/\delta t &= Inuc \cdot n_{h2so4} \cdot m_{h2so4} + C_1 \cdot m_{h2so4}N_{h2so4}N_1 \\
&\quad -K_{12}N_1N_2 \cdot m_{p1} - K_{13}N_1N_3 \cdot m_{p1} - K_{14}N_1N_4 \cdot m_{p1} \\
\delta M_2/\delta t &= C_2 \cdot m_{h2so4}N_{h2so4}N_2 + K_{12}N_1N_2 \cdot m_{p1} \\
&\quad -K_{23}N_2N_3 \cdot m_{p2} - K_{24}N_2N_4 \cdot m_{p2} \\
\delta M_3/\delta t &= C_3 \cdot m_{h2so4}N_{h2so4}N_3 + K_{23}N_2N_3 \cdot m_{p2} - K_{34}N_3N_4 \cdot m_{p3} \\
\delta M_4/\delta t &= C_4 \cdot m_{h2so4}N_{h2so4}N_4 + K_{34}N_3N_4 \cdot m_{p3}
\end{aligned} \tag{A.6}$$

Here M_i (μg m^{-3}) is the SO_4 mass concentration in mode i, n_{h2so4} is the number of sulphuric acid molecules in a critical cluster, m_{h2so4} is the mass of a sulphuric acid molecule, $C_iN_{h2so4}N_i$ (molec/m^{3}s) is the condensation rate of sulphuric acid onto particles in the mode i, m_{pi} is the mass of an average sulphate particle in the mode i. Terms $K_{ij}N_iN_j \cdot m_{pi}$ designate the mass lost from the smaller mode$i$ and gained by the larger mode$j$ due to coagulation between particles in these modes. Evolution equations for the masses of other aerosol component can be written analogously, excluding nucleation and condensation terms.

The prognostic mass equations are formulated for dry masses. Particles containing hygroscopic components (SO_4, NO_3, NH_4, sea salt and partly OC) will change their sizes due to water condensation or evaporation depending on the ambient relative humidity. A current wet diameter D_i of the particles in each size mode is calculated as

$$D_i = \left(\frac{6}{\pi} \cdot \frac{M_i}{\rho_i N_i} \right)^{1/3} \tag{A.7}$$

where M_i is the total, including water component, aerosol mass in the size mode i, ρ_i is the average particle density in the mode i, which is updated at every time step depending on the particle chemical composition. The aerosol water content is a diagnostic parameter and calculated in UNI-AERO by the EQSAM model (see section A.3.2). The actual "wet" diameter is then used in calculations of aerosol dynamics and particle dry deposition.

A.4.1 Nucleation

Nucleation is one of the main processes for new particles production. In the aerosol model, three parameterisations for the rate of particle formation by nucleation are available. Those are:

- Binary nucleation rate based on the revised classical theory for binary homogeneous nucleation for H_2SO_4-H_2O system (Kulmala et al. 1998).
- A preliminary parameterisation for ternary H_2SO_4-NH_3-H_2O nucleation rate developed by Korhonen et al. (1999).
- Parameterisation for the binary nucleation rate formulated at the Institute for Tropospheric Research in Leipzig (Berndt et al. 2000).

An empirical parameterisation for the rate of homogeneous nucleation of H_2SO_4-H_2O from the MADMAcS model at the Institute of Tropospheric Research, Leipzig is currently used in model calculations. A general form for the nucleation rate I_nuc (m^{-3} s^{-1}) is

$$I_{nuc} = (A \cdot [C_{h2so4}]^{na} \cdot [C_{h2o}]^{nw})/(B + [C_{h2o}]^{nw}) \quad \text{(A.8)}$$

where $[C_{h2so4}]$ and $[C_{h2o}]$ are the concentrations of sulphuric acid and water, na and nw are number of sulphuric acid and water molecules in a stable critical cluster, A and B are empirical parameters. The critical H_2SO_4 concentration necessary for nucleation onset is calculated following Kulmala et al. (1998)

$$C_{\text{h2so4,crit}} = \exp(-14.5125 + 0.1335T - 10.5462Rh - 19.85Rh/T) \quad \text{(A.9)}$$

$C_{h2so4,crit}$ is the critical gas-phase H_2SO_4 concentration, which provides a nucleation rate of 1 m^{-3} s^{-1}, T is the temperature and Rh is the fractional relative humidity.

Newly formed particles are assigned to the nucleation mode.

A.4.2 Condensation

Condensation of vapours is one of the processes responsible for the growth of atmospheric particles, especially nucleation and Aitken, and for changing the aerosol chemical composition. Condensation is driven by the difference between ambient gas

concentration and that at the particle surface. In MM32, only condensation of gaseous H_2SO_4 is presently considered. H_2SO_4 vapour pressure at the particle surface is currently assumed to be zero, which will result in maximum condensation flux. The continuum regime theory for condensation corrected for the free-molecular regime by a transitional correction factor is used to calculate the condensation rate (Fuchs and Sutugin 1970). The expression for condensation rate C_{cond}(molec m^{-3} s^{-1})of H_2SO_4 to particles in mode i is written as

$$C_{cond} = C_i N_{h2so4} N_i \tag{A.10}$$

where $C_i = 4\pi \cdot r_i \beta_M D$. Here, N_{h2so4}(cm^{-3}) is the concentration of sulphuric acid molecules, N_i (cm^{-3}) is the number concentration and r_i is the radius of particles in mode i, D is the diffusion coeffi cient. β_M is the transition correction factor calculated as

$$\beta_M = \frac{Kn + 1}{0.377Kn + 1 + \frac{4}{3}\alpha^{-1}Kn^2 + \frac{4}{3}\alpha^{-1}Kn} \tag{A.11}$$

where α is the accommodation coeffi cient (presently α=1), $Kn = \lambda_v/r$ is the Knudsen number, λ_v is the mean free path of vapour molecules. In the continuum regime (Kn <=1), β_M =1 and in the free-molecular regime (Kn >10), $\beta_M \sim 3d/(4\lambda_v)$.

A.4.3 Coagulation

Coagulation modifi es the aerosol size distribution, and its overall effect is a reduction of particles number. This process is particularly effi cient for smallest particles in the nucleation and Aitken modes. Currently, only coagulation due to particle Brownian motion, which is the dominating coagulation mechanism for sub-micron particle, is accounted for in UNI-AERO. MM32 calculates the Brownian coagulation coeffi cients based on Fuchs (1964). The Brownian coagulation coeffi cient K_{ij} (cm^{-3} s^{-1}) between particles in i and j modes is calculated for all size regimes, i.e. free molecular (Kn >10), transition (1< Kn <=10) and continuum (Kn <=1) by

$$K_{ij} = \frac{K_C^B}{\frac{r_i + r_j}{r_i + r_j + \sigma_{ij}} + \frac{4(D_i + D_j)}{(\bar{c}_i^2 + \bar{c}_j^2)^{1/2}(r_i + r_j)}} \tag{A.12}$$

where the Brownian coagulation coeffi cient in the continuum regime is:

$$K_C^B = 4\pi(r_i + r_j)(D_i + D_j) \tag{A.13}$$

Here r_i and r_j are the radii of coagulating particles, D_i and D_j are their diffusion coeffi cients, and $\bar{c}_i$ is the particle mean termal velocity. The coagulation coeffi cient is smallest for particles of the same size and increases rapidly as the ratio between the particle diameters increases.

When intermodal coagulation occurs, particles from the smaller mode coagulate to particles in the larger mode. If coagulating particles belong to the same mode (intramode coagulation) they will continue in the same mode after coagulation.

A.4.4 Mode merging

The scheme for aerosol mass transfer from the nucleation to the Aitken mode and from the Aitken to the accumulation mode due to particle growth is based on the "mode merging by renaming" algorithm by Binkowski (1999). To apply this method, a log-normal particles size distribution is imposed on the nucleation and Aitken mode. Constant values for standard deviations of particle distribution are assigned in these modes based on observation data (e.g. Jaenicke (1993), Neusüß et al. (2002)).

The criterion for mode merging used is

$$\sigma_g d_g > d_{th}$$

where d_g is the geometric mean diameter, which is equal to the monodisperse diameter, and σ_g is the geometrical standard deviation for the log-normal distribution, and d_{th} is the threshold upper diameter. The complementary error function for particle number and mass is then used to find the fractions of particles greater than the threshold value as:

$$F_N = 0.5 \cdot erfc(x_N), \qquad F_M = 0.5 \cdot erfc(x_M) \tag{A.14}$$

where F_N and F_M are the fractions of particle number and mass to be moved to the larger mode, and

$$x_N = \frac{\ln\left({}^{D_l}/_{Dg}\right)}{\sqrt{2}\ln\sigma_g}, \qquad x_M = x_N - \frac{3\ln\left(\sigma_g\right)}{\sqrt{2}} \tag{A.15}$$

Then, the correspondent portions of number and mass concentrations (including aerosol water) transferred to the larger mode, and the diameters in both modes are re-calculated based on new mass and number concentrations.

A.5 Aerosol water content

The aerosol associated water is treated in the aerosol model as a diagnostic parameter and calculated by the equilibrium model EQSAM (see section A.3.2) as:

$$LWC = \sum_{i}^{N} (M_i/m_i) \tag{A.16}$$

where LWC is the aerosol liquid water content (kg m^{-3}), N is the total number of single-salt solutions, M_i [mol/m^3] is the molar concentration and m_i [mol/kg] is the molality of salt i.

Aerosol water in each size mode is computed at every time step and added to the particle dry mass. Based on the total PM mass, the particle "wet" diameters are derived and then used in the aerosol dynamics and in the dry and wet deposition calculations. Consistently, the particle density is re-calculated as the mass weighted average of the densities of all (including aerosol water) aerosol components in each mode.

A.6 Cloud processing of aerosols

A.6.1 Accumulation particles

In clouds, all particles in the accumulation mode are assumed to get activated and form cloud droplets. This provides the medium for aqueous oxidation of SO_2 by H_2O_2 and O_3 for form sulphate aerosol (see section A.3.1), resulting in the growth of accumulation particles. Presently in the aerosol model, 95% of SO_4 formed in clouds goes to increase the mass in accumulation mode.

A.6.2 Aitken particles

The part of Aitken particles, which radii exceed the critical radius at the actual supersaturation, get activated and assumed to grow fast enough to the accumulation mode. A simple preliminary relationship from Fitzgerald (1973) between dry critical radius and the supersaturation is implemented in UNI-AERO:

$$r_d = 1.53 \cdot 10^{-6} \varepsilon^{-0.31} S_c^{-2/3} \tag{A.17}$$

where r_d (cm) is the particle dry critical radius, ε is the fraction of water-soluble species in the particle (0.3 and 0.5 values were tested), and Sc (%) is the supersaturation. To obtain the fraction of Aitken particles with radius greater than r_d, a log-normal size distribution is imposed on Aitken particles in the same way as in section A.4.4.

The remaining portion of Aitken aerosols becomes interstitial cloud aerosols, which contain a signifi cant amount of water thus facilitating aqueous phase reactions. 5% of SO_4 formed in aqueous reactions goes to grow Aitken particles (H.-C. Hansson, person. comm.).

A.7 Dry deposition

The common formulation for parameterisation of dry deposition of gases and particles is employed in the Unifi ed model and in the aerosol model (see section 8). The only difference is that the actual particle sizes, i.e. wet diameters, are used to calculate dry deposition velocities of particles in each mode.

Table A:3: Particle in-cloud scavenging ratio (W_{in}) and sub-cloud collection effi ciency (E) presently used in UNI-AERO

	nucleation mode	Aitken mode	Accumulation mode	coarse mode
$W_{in} \cdot 10^6$	0.0	0.2	0.7	0.7
E	0.4	0.3	0.1	0.4

A.8 Wet scavenging

The common parameterisations of wet deposition of gases and particles are employed in the Unifi ed model and the aerosol model (see section 9). The only difference is that in UNI-AERO, the in-cloud scavenging ratios and the collection effi ciencies for below-cloud aerosol scavenging are assigned in each size mode (Table A:3). The correspondent scavenging rates are applied for both particle number and mass concentrations in each mode.

References

Y. Andersson-Sköld and D. Simpson. Secondary organic aerosol formation in Northern Europe: a model study. *J. Geophys. Res.*, 106(D7):7357–7374, 2001.

J. J. M. Berdowski, W. Mulder, C. Veldt, A. J. H. Vesschedijk, and P. Y. J. Zandved. Particulate matter emissions (PM10-PM2.5-PM0.1) in Europe in 1990 and 1993. Technical report, Netherlands organisation for Applied Scientifi c Reaserch, 1997. TNO-MEP-R 96/472, Apeldoorn, the Netherland.

T. Berndt, O. Böge, T. Conrath, F. Stratmann, and J. Heitzenberg. Formation of new particles in the system $H_2SO_4(SO_3)$ / H_2O / (NH_3) – fi rst results from a flow-tube study. *J. Aeros. Sci.*, 31(Suppl. 1):S554–S555, 2000.

J. W. Fitzgerald. Dependence of the Supersaturation Spectrum of CCN on Aerosol Size Distribution and Composition. *J. of Atmospheric Sciences*, 30:628–634, 1973.

N. A. Fuchs. *The mechanics of aerosols*. Pergamon Press, London, 1964.

N. A. Fuchs and A. G. Sutugin. *Highly dispersed aerosol*. Ann. Arbor Science Publ., Ann Arbor Michigan, 1970. p.105.

R. Jaenicke. Tropospheric aerosols. In P. V. Hobbs, editor, *Aerosol-Cloud-Climate interactions*, pages 1–31. Academic Press, San Diego, CA, 1993.

P. Korhonen, M. Kulmala, A. Laaksonen, Y. Viisanen, R. McGraw, and J. H. Seinfend. Ternary nucleation of H_2SO_4, NH_3 and H_2O in the atmosphere. *J. Geophys. Res.*, 104:26349–26353, 1999.

M. Kulmala, A. Laaksonen, and L. Pirjola. Parameterization for sulfuric acid/water nucleation rates. *J. Geophys. Res.*, 103:8301–8308, 1998.

E. M. Mårtensson, E. D. Nilsson, G de Leeuw, L. H. Cohen, and H.-C. Hansson. Laboratory simulations and parameterization of the primary marine aerosol production. *J. Geophys. Res.*, 108, 2003. doi:10.1029/2002JD002263, in press.

F. J. Metzger, S. M. andDentener, J. Lelieveld, and S. N. Pandis. Gas/aerosol partitioning: I. A computationally effi cient model. *J. Geophys. Res.*, 107(D16), 2002. doi:10.1029/2001JD001102, 2002.

E. C. Monahan, D. E. Spiel, and K. L. Davidson. A model of marine aerosol generation via whitecaps and wave disruption. In E. C. Monahan and G. MacNiochaill, editors, *Oceanic Whitecaps*. D. Reidel, Norwell, Mass., 1986.

C. Neusüß, H. Wex, W. Birmili, A. Wiedensohler, C. Koziar, B. Busch, E. Brüggemann, T. Gnauk, M. Ebert, and D.S. Covert. Characterisation and parameterization of atmospheric particle number-, mass-, and chemical-size during LACE 98 and MINT. *J. Geophys. Res.*, 107(D21), 2002. doi:10.1029/2001JD000514, 2002.

L. Pirjola and M. Kulmala. Aerosol dynamical model MULTIMONO. *Boreal Environ. Res.*, 5:361–374, 2000.

L. Pirjola, S. Tsyro, L. Tarrasón, and M. Kulmala. A monodisperse aerosol dynamics module, a promising candidate for use in long-range transport models: Box model tests. *J. Geophys. Res.*, 108(D9), 2003. doi:10.1029/2002JD002867, 2003.

J.H. Seinfeld and S.N. Pandis. *Atmospheric chemistry and physics. From air pollution to climate change* . John Wiley and Sons, inc., New York, 1998.

APPENDIX B

Calculations of AOTx and Stomatal Flux

B.1 Introduction

One of the main reasons for running the EMEP model is to generate results for use in intergrated assessment modelling (IAM), and for studies on the risks and damages caused by pollution. In previous years the ozone outputs have consisted largely of so-called AOTx values (typically AOT40, AOT60) which were based upon the model's predicted grid-average ozone concentrations at a height [1] of 1 m.

New concepts for assessing risks of damage to vegetation have meanwhile been developed and incorporated into the new ICP Mapping Manual (see UNECE 2003, and references therein).

The first important change is that the Mapping Manual now places extra stress on the need to calculate ozone concentrations at the top of the vegetation canopy, rather than to some height above the canopy (e.g. 1 m, as typically used in modelling, or 3-5 m as often used from measurements). Thus, AOTx calculations should now be specific to the vegetation in question rather than just grid-square averages as calculated previously.

Additionally, the Mapping Manual has now defined critical levels for ozone uptake though the stomata of vegetation - a much more ambitious undertaking, but one for which there are strong biological arguments. The Mapping Manual suggests three vegetation categories for which stomatal flux calculations should be conducted. These are wheat, potato and beech.

These new concepts have lead to a need for more complex outputs from the EMEP model, and this Appendix outlines the new outputs and their derivation in the model. It should be noted that not only stomatal fluxes, but also the canopy-level concentrations,

[1] Technically, the calculations were to a height 1 m above the displacement height of the model grid

AOTs, and fluxes are inherently more uncertain than calculations of concentrations at levels such as 3 m above the canopy or of boundary layer averages. However, the potential benefits of calculating ozone close to the canopy, from the effects point of view, hopefully outweigh the uncertainties involved.

It should be emphasised that no final decisions have yet been made on the outputs to be used in IAM modelling for policy purposes. However, the methods outlines below are intended to be flexible (for example in the choice of growing seasons, parameters) and hopefully cover most requirements.

B.2 Ozone concentrations at the canopy height

If we have modelled concentrations $c(z_R)$ at reference height z_R, then we find concentration values appropriate to a height z_1 (1 m, say) by making use of the constant-flux assumption and definition of aerodynamic resistance:

$$\text{Total flux} = V_g(z_R).c(z_R) = (c(z_R) - c(z_1))/R_{a,h}(z_R, z_1) \tag{B.1}$$

where $V_g(z_R)$ is the deposition velocity (m/s) at height z_R, and $R_{a,h}(z_R, z_1)$ is the aerodynamic resistance for heat and scalars between the two heights (s m^{-1}). Rearranging the 2nd two terms, we get:

$$c(z_1) = c(z_R).[1 - (R_{a,h}(z_R, z_1).V_g(z_R))] \tag{B.2}$$

The deposition velocity, V_g, and resistance $R_{a,h}(z_R, z_1)$ are calculated as described in chapter 8, eqns [8.2] and [8.8].

B.3 Calculation of AOTx

The accumulated amount of ozone over a threshold value of x ppb is defined as:

$$AOTx = \int max(c - x, 0.0)\, dt \tag{B.3}$$

where the max function excludes negative values. The integral is taken over time, and varies with the critical level under consideration. For UNECE critical levels, only daylight values are counted - in the model we approximate this as hours when the solar zenith angle is 87° or less. For EU purposes, AOT40 is defined over a fixed hourly period - from 0800-2000 Central European Time.

For crops and natural vegetation AOT40 is generally calculated over 3 months (previously May-July). For forests a six month period is used (April-September). AOT60 has been used as an indicator of health-related effects, and for this purpose the integral is taken over 6 months. At the time of writing it is not clear how growing seasons will be defined for use in intergrated assessment modelling, but since the model calculates ozone over typically a full year then outputs can be tailored to suit a variety of needs.

B.4 Stomatal Flux Calculations

The estimation of stomatal flux of ozone (F_{st}) is based upon the assumption that the concentration of ozone at the top of the canopy represents a reasonable estimate of the concentration near the sunlit upper canopy leaves (or flag leaf in the case of wheat), at the upper surface of the laminar layer. If $c(h)$ is the concentration of ozone at canopy top (height h, unit: m), in nmol m^{-3}, then F_{st} is given by:

$$F_{st} = c(h) \frac{1}{r_b + r_c} \frac{g_{sto}}{g_{sto} + g_{ext}} \tag{B.4}$$

Units for F_{st} are nmol m^{-2} PLA s^{-1}, where PLA is projected leaf area (m^2 m^{-2}). The $1/(r_b + r_c)$ term represents the deposition rate to the leaf through resistances r_b (quasi-laminar resistance) and r_c (leaf surface resistance). The fraction of this ozone taken up by the stomata is given by $g_{sto}/(g_{sto} + g_{ext})$, where g_{sto} is the stomatal conductance, and g_{ext} is the external leaf, or cuticular, conductance. As the leaf surface resistance, r_c, is given by $r_c = 1/(g_{sto} + g_{ext})$, we can also write eqn B.4 as:-

$$F_{st} = c(h)\ g_{sto} \frac{r_c}{r_b + r_c} \tag{B.5}$$

A value for g_{ext} has been chosen to keep consistency with the bulk canopy values evaluated in previous EMEP model versions:

$$g_{ext} = 1/2500 \qquad \text{(m s}^{-1}\text{)}. \tag{B.6}$$

Consistency of the quasi-laminar boundary layer is harder to achieve, so the use of a leaf-level r_b term (McNaughton and van der Hurk 1995) is suggested, making use of the cross-wind leaf dimension L_d and the wind speed at height h, $V(h)$:

$$r_b = 1.3 \times 150 \sqrt{\frac{L_d}{V(h)}} \tag{B.7}$$

with units s m^{-1}. The factor 1.3 accounts for the differences in diffusivity between heat and ozone. $V(h)$ is calculated from the model's grid-centre wind speed by application of standard similarity functions for momentum. The model currently uses L_d=2 cm for wheat and potato, and 4 cm for deciduous forests.

The core of the leaf ozone flux model is the stomatal conductance (g_{sto}) multiplicative algorithm which has been developed over the past few years and incorporated within the EMEP ozone photochemical modelling framework (Emberson et al. 2001, 2000a,b, Simpson et al. 2000, 2001, 2003, Tuovinen et al. 2001, 2003). The multiplicative algorithm is identical to that used for the bulk canopy calculations (chapter 8,eqn [8.13]):

$$g_{sto} = g'_{max} . f'_{phen} . f'_{light} . \max\{f'_{min}, f'_T . f'_{VPD} . f'_{SWP}\} \tag{B.8}$$

except that g_{max} and the f-factors, here denoted f', can be defined differently for upper-canopy leaves and for integrated assessment modelling than for the bulk-canopy modelling used in normal deposition calculations.

B.5 Modelling for Wheat, Potato and Beech

Although there are obvious links between modelling of stomatal fluxes (F_{st}) for Critical Levels calculations and modelling for deposition purposes, these calculations have important differences. The F_{st} values represent maximum uptake to a small portion of the canopy, not net uptake to the whole canopy. These F_{st} calculations are therefore performed as a parallel excercise and some articial features are introduced in order to provide more useful output for IAM purposes.

Firstly, wheat, potato and beech are treated for F_{st} modelling as 'artificial' species which do not affect the general dry deposition applied within the EMEP model - their effects on deposition are already taken account of in a realistic way through the categories temperate crops, root crops and deciduous forests (chapter 8). In order to allow for the possibility of these crops or beech forests growing anywhere within the grid (i.e. allowing for the possibility that the landuse maps may not be 100% accurate in this respect), these artificial categories are added as a tiny fraction of each grid square where any vegetation is present.

Table B:1 lists the values of the parameters used for these three vegetation categories. In general the functions used are similar to those of the deposition calculations except:

f_{temp} : an asymmetric form for the temperature function, f_{temp}, is introduced:

$$f'_{temp} = \frac{T - T_{min}}{T_{opt} - T_{min}} \left[\frac{T_{max} - T}{T_{max} - T_{opt}} \right]^{bt} \tag{B.9}$$

where $bt = (T_{max} - T_{opt})/(T_{opt} - T_{min})$.

f_{light} : as Emberson et al. (2000b) but only sunlit leaves are used in the calculation

g_{max} : The conductance values for wheat and potato are higher than the values used for the generic temperate crop and root crop classes. These higher values are based upon a a review of recent literature for the crops in question (UNECE 2003, Karlsson et al. 2003).

More fundamental changes are implemented for the growing season and phenology functions for wheat and potatoes, because of the rather short time-periods for which these crops are sensitive to ozone. These biologically determined time-windows are difficult to identify using large-scale modelling, since they will vary considerably with climate, altitude, year-to-year meteorology and agricultural practice. In addition, use

of short-time periods leads to the risk of missing events where ozone concentrations are high. Given these uncertainties in the timing of this period, UNECE (2003) recommended an alternative approach for IAM purposes upon which our implementation is based.

For these crop species, a fi xed value of the phenology factor f_{phen} of 0.8 is applied continuously. LAI is set at the maximum value over this time period, with SAI set accordingly to LAI+1.5 (see eqn [8.19]).

F_{st}, and associated $F_{st}Y$ values (fluxes exceeding a desired flux threshold Y) are then calculated continuously and output from the model on a daily basis. This then allows post-processing of the data to obtain the period of maximum accumulated 30-day $F_{st}Y$, denoted $AF_{st}Y$, during a 3-month growing season, as recommended bu UNECE (2003).

For beech forests, with a growing season of typically 6 months, the procedures are much simpler and standard values of LAI, SAI, f_{phen}, etc. are identical to those of temperate deciduous forests. $F_{st}Y$ are then straightforwardly available, either on a daily basis or on a 6-monthly basis.

Table B:1: Parameters used for Critical Level Modelling

	Units	Wheat	Potato	Beech
g'_{max}	mmole O_3 m^{-2} PLA s^{-1} , (a)	450	750	134
f'_{min}	fraction	0.01	0.01	0.13
SGS	day number	(b)	(b)	90
EGS	day number	(b)	(b)	270
f_{phen}	fraction	0.8	0.8	(c)
α (in f_light)	fraction	0.0105	0.005	0.006
T_{min}	°C	12	13	-5
T_{opt}	°C	26	28	22
T_{max}	°C	40	39	35
VPD_{max}	kPa	1.2	2.1	0.93
VPD_{min}	kPa	3.2	3.5	3.4
SWP_{max}	MPa	-0.3	-0.5	-0.05
SWP_{min}	MPa	-1.1	-1.1	-1.5

Notes: (a) Conversion of g'_{max} as given here to units of m s^{-1} is done using equation [8.14] (b) Movable growing seasons - see text (c) function used as for deciduoius forest (DF) in Table 8.1 For more details, see UNECE (2003), Karlsson et al. (2003).

References

L. Emberson, M.R. Ashmore, H.M. Cambridge, D. Simpson, and J.P. Tuovinen. Modelling stomatal ozone flux across Europe. *Environmental Pollution*, 109(3):403–414, 2000a.

L. Emberson, D. Simpson, J.-P. Tuovinen, M.R. Ashmore, and H.M. Cambridge. Towards a model of ozone deposition and stomatal uptake over Europe, 2000b. EMEP MSC-W Note 6/2000.

L.D. Emberson, M.R. Ashmore, D. Simpson, J.-P. Tuovinen, and H.M. Cambridge. Modelling and mapping ozone deposition in Europe. *Water, Air and Soil Pollution*, 130:577–582, 2001.

P.E. Karlsson, Selldén, and H. Pleijel, editors. *Establishing Ozone Critical Levels II. UNECE Workshop Report, Gteborg, Sweden, 19-22 November, 2002*, 2003. IVL, Swedish Environmental Research Institute. IVL Report B 1523.

K.G. McNaughton and B.J.J.M. van der Hurk. 'Lagrangian' revision of the resistors in the two-layer model for calculating the energy budget of a plant canopy. *Boundary Layer Meteor.*, 74:261–288, 1995.

D. Simpson, L. Emberson, J.P. Tuovinen, and M. Ashmore. Ozone deposition and stomatal flux modelling, 2000. In EMEP Report 2/2000, Transboundary Photooxidants in Europe. Norwegian Meteorological Institute, Oslo, Norway.

D. Simpson, J.-P. Tuovinen, L.D. Emberson, and M.R. Ashmore. Characteristics of an ozone deposition module. *Water, Air and Soil Pollution, Focus*, 1:253–262, 2001.

D. Simpson, J.-P. Tuovinen, L.D. Emberson, and M.R. Ashmore. Characteristics of an ozone deposition module ii: sensitivity analysis. *Water, Air and Soil Pollution*, 143: 123–137, 2003.

J.-P. Tuovinen, M.R. Ashmore, L.D. Emberson, and D. Simpson. Testing and improving the EMEP deposition module, 2003. Submitted.

J.-P. Tuovinen, D. Simpson, T.N. Mikkelsen, L.D. Emberson, M. R. Ashmore M., Aurela, H. M. Cambridge, M. F. Hovmand, N. O. Jensen, T. Laurila, K. Pilegaard, and H. Ro-Poulsen. Comparisons of measured and modelled ozone deposition to forests in Northern Europe. *Water, Air and Soil Pollution, Focus*, 1:263–274, 2001.

UNECE. International Cooperative Programme on Modelling and Mapping of Critical Loads & Levels and Air Pollution Effects, Risks and Trends. Manual on Methodologies and Criteria for Mapping Critical Levels/Loads and geographical Areas where they are exceeded, 2003. To be published. See `www.oekodata.com/icpmapping/html/manual.htm`.